The landscape model: a model for exploring trade-offs between agricultural production and the environment

Journal: Science of the Total Environment

The Landscape Model: a model for exploring trade-offs between agricultural production and the environment.

Kevin Coleman[a*], Shibu E. Muhammed[a], Alice E. Milne[a], Lindsay C. Todman[a], A. Gordon Dailey[a], Margaret J. Glendining[b], Andrew P. Whitmore[a]

[a] *Sustainable Agriculture Sciences department,* [b] *Computational and Analytical Sciences department, Rothamsted Research, Harpenden, Hertfordshire, AL5 2JQ, UK*

Keywords: Modelling, crops, soil processes, nutrient flow, water movement, agriculture

*Corresponding author

E-mail address alice.milne@rothamsted.ac.uk

HIGHLIGHTS

- Understanding trade-offs between yield and environment is essential for SI
- The Landscape Model aids the understanding of crop-soil-water interactions
- Model validated against 50 years of data from two long-term experiments
- Model validated against spatially-explicit data from the North Wyke farm platform
- The model simulated wheat yield, grain N and grain P particularly well

ABSTRACT

We describe a model framework that simulates spatial and temporal interactions in agricultural landscapes and that can be used to explore trade-offs between production and environment so helping to determine solutions to the problems of sustainable food production. Here we focus on models of agricultural production, water movement and nutrient flow in a landscape. We validate these models against data from two long-term experiments, (the first a continuous wheat experiment and the other a permanent grass-land experiment) and an experiment where water and nutrient flow are measured from isolated catchments. The model simulated wheat yield (RMSE 20.3-28.6%), grain N (RMSE 21.3-42.5%) and P (RMSE 20.2-29% excluding the nil N plots), and total soil organic carbon particularly well (RMSE $3.1 - 13.8\%$), the simulations of water flow were also reasonable (RMSE 180.36 and 226.02). We illustrate the use of our model framework to explore trade-offs between production and nutrient losses.

GRAPHICAL ABSTRACT

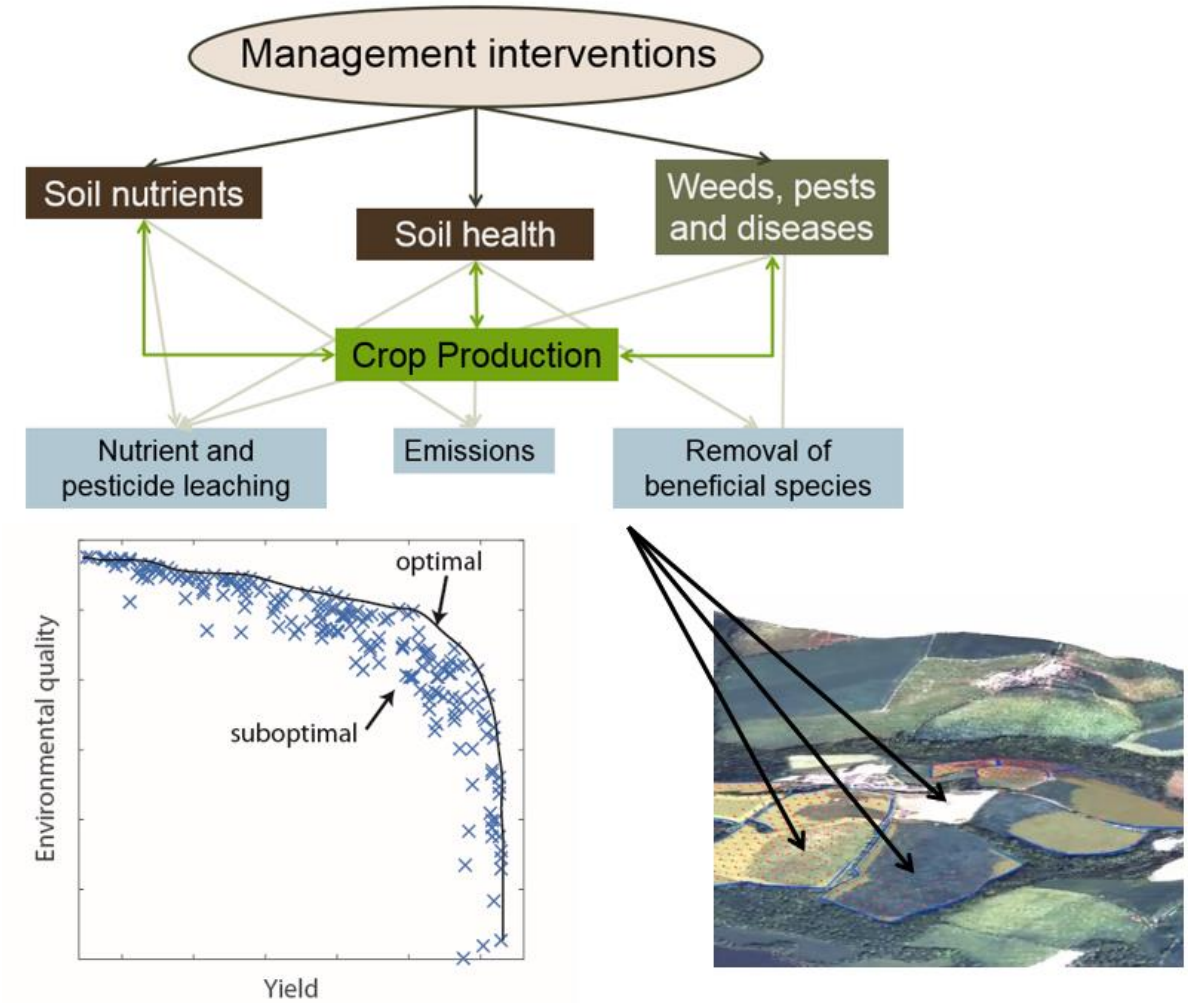

1. Introduction

Increasingly, agricultural production is being compelled to look not just at its externalities such as the environmental pollution or depletion of natural resources but also at the provision of wider ecosystem services such as biodiversity. Schemes to monitor or assess land for all of these factors are prohibitively expensive and yet there is a need to analyse modern agricultural systems for the purposes of policy, planning or management. Not surprisingly therefore, computer simulation models have a role to play in filling the large gaps between what we need to know and what is available from measurements.

Simulation models of agricultural systems abound, some focussing on specific aspects such as soil organic matter dynamics (Coleman et al., 1997), crop growth (Semenov and Stratonovitch, 2015), water movement (Addiscott and Whitmore, 1991), emissions (Rolston et al., 1984), competing organisms (Andrew and Storkey, 2017), and some integrating to agricultural management systems (Brisson et al., 2003; Keating et al., 2003). Others focus on the natural systems, tracing biodiversity often quite specifically (Andam et al., 2008; Koh et al., 2010). Some models, particularly agricultural ones, focus on field (Bell et al., 2012; Parton et al., 1994) or farm scales (Del Prado et al., 2011). Biodiversity models often focus on larger scales and water management models are naturally focussed on river basins or catchments (Whitehead et al., 2014).

Many models simulate fields or regions, some simulate particular fluxes, say water from land to rivers. It is rarer to find models that try to integrate several of the impacts of farming in the landscape, and those that do adopt a relatively empirical, data-driven approach (Jackson et al., 2013; Tilman et al., 2001) that makes it difficult to explore the interactions between components of that landscape that might be better managed with a more holistic overview. It is rarer still to find models that make explicit spatial and temporal linkage between

adjacent fields and integrate all aspects of the managed farm environment up to the catchment level. Such a model would be useful to understand the spatial interactions and impact of the natural (weeds, pest and diseases) as well as management (irrigation, fertilizer and application of pesticides) events on an agricultural landscape. Our aim is to develop a spatially explicit model that can simulate the essential processes of soil, water, crop growth and biodiversity for agricultural landscapes in the UK. This model can then be used to understand the trade-off between farm management practices on farm economy and the environment. The ability to quantify such trade-offs is critical to our management of the landscape and underpins many sustainability frameworks including the three pillars of sustainability (environmental, economic and social), the UN Sustainable Development goals which includes several targets that relate to agricultural landscapes (Gil et al., 2017), and water-energy-food nexus approaches that aim to consider the use of all of these resources. While tradeoff models exist (e.g. see Sharps et al., 2017) they usually operate at large scales, not accounting for the field or farm scale at which land management decisions are often made. These models are often focussed on land-use options within in GIS-based systems, operate on annual time-scales and can be focussed on policy. Our approach, and ultimate aim, is to simulate interactions between the multiple processes that take place in agricultural fields and the farmed landscape with a view to uncovering strategies for development and improvement of agri-environmental systems, beyond the current envelope (Fig 1). By working on a daily time-step we can simulate the processes and inform the decisions that someone who manages land will have to take.

Here we report the first version of our model that integrates agricultural production, water movement and nutrient flow in a landscape. The model combines aspects of several published model [RothC (Coleman and Jenkinson, 2014), LINTUL (Wolf, 2012), SUCROS (van Laar et al., 1997), and Century (Parton et al., 1994)], but also includes novel factors that have been implemented to capture potential improvements in yield that result from

management actions. These include coupling the RothC model to include the dynamics of N and P and responses to changes in bulk-density that result from changes in soil organic matter. We evaluate the model against data on crop growth and nutrient uptake for cereals and for grass, and the integration in space of water and nutrients leaving agricultural fields. We then illustrate how our model can be used to explore trade-offs between production and environment with a scenario based on a wheat crop grown in conditions typical of arable England.

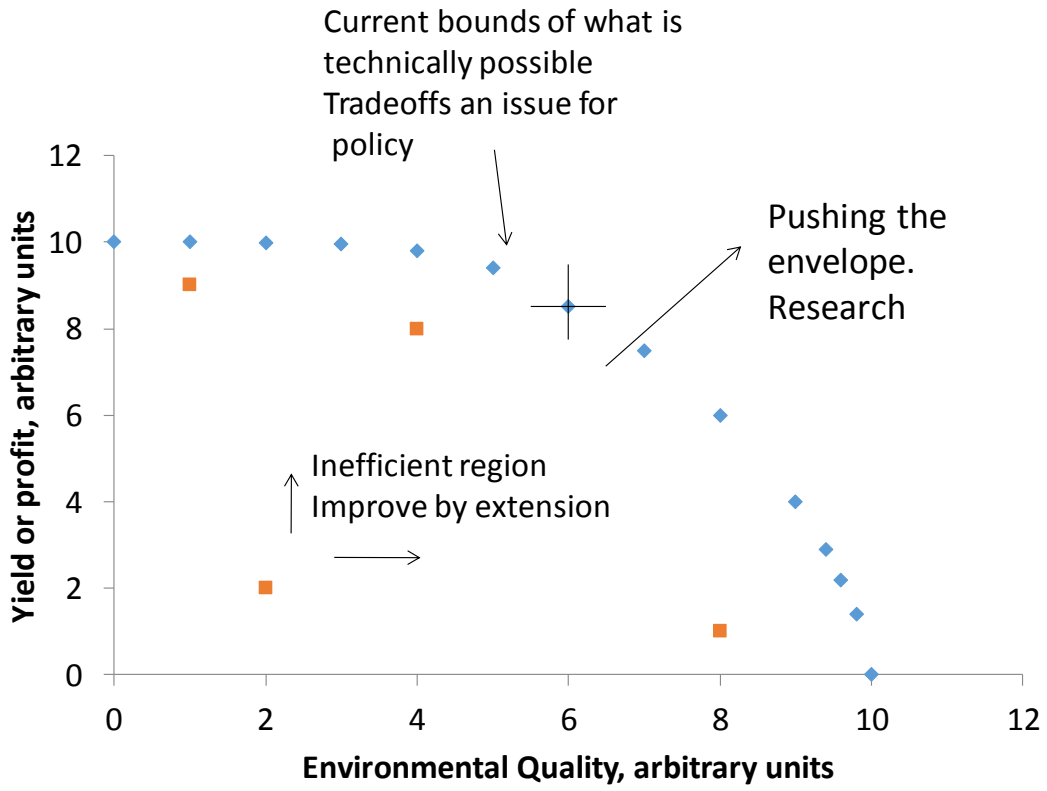

Fig1: Representation of an environmental-economic production possibility frontier. The blue diamonds are independent outcomes of management that optimises both yield and environmental quality at the same time. A decision along this line is a matter for policy. The orange squares within the envelope are inefficient in the sense that either production or environmental quality could be improved without impacting the other. This is the region for extension. Beyond the envelope is a zone where outcomes are currently infeasible and this is

the area which research addresses. An origin placed over any point (for example the cross shown in the figure on the middle of the envelope), facilitates the definition of the envelope algorithmically: if another point can be found in the first quadrant (North East) then the first point in not on the envelope.

2. Methodology

Our intention was to build a model system capable of exploring the multiple interactions between components of a simple landscape and to take into account both within and between field movement of components such as water and nitrate. Nonetheless, because we wished to build a system that can be used on a reasonably large landscape comprising many fields and boundaries, we based our system on simple but adequate descriptions of the processes involved. Here we report on interactions and differences between single or adjacent but joined fields and focus our discussion on productivity and loss of water and nitrogen to water courses and the atmosphere. To do so we describe an integrated model of crop, water and soil processes that runs on a daily time step. We validate this using data from the Broadbalk and Park Grass long-term experiments at Rothamsted Research, in Harpenden, SE England, and spatial interactions are tested on data from the more recently established North Wyke Farm Platform, at Rothamsted Research, near Okehampton, SW England (Orr et al., 2016).

2.1 Spatial structure

We impose a grid on the landscape where, dependant on size, each field is represented by one or more grid cells. Soil properties are set in each cell and initial values are given for bulk density, pH and soil water. Within each cell we model crop growth, the dynamics of soil water, total soil organic carbon (TOC), changes in bulk density and nutrient flows on a daily

time step. In cases where fields are made up of several cells, water and nutrients can move laterally between cells, as well as vertically though the soil profile. This model structure allows us to explore both temporal and spatial interactions. Cell edges can be designated as ditches (into which water and nutrients may flow), hedgerows or field margins.

2.2 *Soil water*

The soil water model uses a capacity based approach (Addiscott and Whitmore, 1991; Van Ittersum et al., 2003; van Laar et al., 1997). The soil is divided into three layers. This choice is a compromise between capturing the heterogeneity of the soil profile (which would require multiple layers in the simulation) and minimising complexity to enable fast run-times which are important when coupling models with optimisation algorithms over large spatial scales. In our study each layer was initially set to 230mm. The capacity of each of the soil layers is calculated with van Genuchten (1980) soil water release curves determined using the HYPRES pedo-transfer functions (Wösten et al., 1999). These functions use texture, soil organic matter and bulk density to derive the water release curves. For the topsoil, these release curves are updated daily to take into account changes in bulk density, for example, when farmyard manure (FYM) is added (see section 2.6).

Infiltrating water fills the soil layers to field capacity (-10 kPa), and starting from the top layer, excess water drains to the layer below, with water draining from layer 3 becoming drainage. In addition to percolation, water is lost by runoff and evaporation from the soil surface, and transpiration by the growing crop. The water available for crop uptake at any time is equal to the quantity of water stored above wilting point (-1500 kPa) in the rooted soil profile. A detailed description of the soil water model can be found in van Laar et al. (1997), with our modifications described in section 2.7. The change in water content in each layer is derived

154 from the balance between inputs from precipitation, and outputs from drainage, runoff,
155 evaporation and transpiration.

156 Working at the water catchment scale Bell et al. (2007) developed a simple algorithm
157 for estimating the total surface water leaving a sloping (i.e. not uniform in the vertical
158 dimension) region. The storage capacity (*S*) of high zones is reduced in relation to the
159 topographic gradient according to

160 $$S = \left(1 - \frac{\bar{g}}{g_{\max}}\right) S_{\max} \quad 1$$

161 where $S_{\max}$ is the maximum storage capacity, $\bar{g}$ is the average gradient in the cell and $g_{\max}$ is
162 the upper limit on the gradient. By adopting this strategy on a grid cell basis, we increase the
163 flow of water out of each cell compared to that if it were flat. Runoff moves from the highest
164 cell to the lowest by moving between cells with neighbouring boundaries. The proportion of
165 runoff allocated in each direction is determined by the relative magnitude of the downward
166 slopes. Dissolved substances such as nitrate, move in proportion to the water.

167

168 2.3 *Soil total organic carbon, nitrogen and phosphorus*

169 The soil total organic carbon (TOC) model is based on the Rothamsted carbon model,
170 RothC, (Coleman and Jenkinson, 2014). Soil total organic carbon is split into four active
171 compartments and a small amount of inert organic matter (IOM). The four active compartments
172 are Decomposable Plant Material (DPM), Resistant Plant Material (RPM), Microbial Biomass
173 (BIO) and Humified Organic Matter (HUM). Each compartment decomposes by a first-order
174 process with its own rate constant. The IOM compartment is resistant to decomposition.
175 Decomposition of each of the four active pools is modified by rate modifying factors for

176 temperature, moisture and plant retainment. Full details of the model can be found in (Coleman
177 and Jenkinson, 2014).

178 The dynamics of the soil organic nitrogen (SON) and phosphorus (SOP) are modelled
179 in a similar way to the TOC dynamics, both SON and SOP have the same pool structure as the
180 active TOC pools. To determine initial values for each TOC pool, the model is run to
181 equilibrium so that the modelled TOC matches the initial measured TOC. The initial values of
182 each of the SON and SOP pools are then determined using the TOC values, and the C:N and
183 C:P ratios of each pool. The $C:N_{\mathrm{Bio}}$ and $C:N_{\mathrm{Hum}}$ ratios are both fixed at 8.5 (Bradbury et al.,
184 1993), whereas $C:N_{\mathrm{DPM}}$ and $C:N_{\mathrm{RPM}}$ ratios vary over time depending on the carbon inputs to
185 soil from the crop or the addition of organic amendments. The $C:P_{\mathrm{Bio}}$ and $C:P_{\mathrm{Hum}}$ ratios are
186 fixed at 50.0 and 100.0 respectively, like nitrogen the $C:P_{\mathrm{DPM}}$ and $C:P_{\mathrm{RPM}}$ ratios vary over
187 time depending on the carbon inputs to the soil from the crop or the addition of organic
188 amendments.

189 The N in pool i that is mineralised or immobilized is given by

190 $$M_i = \frac{\Delta_i}{\rho_i} - \frac{B_i}{\rho_{\mathrm{Bio}}} - \frac{U_i}{\rho_{\mathrm{Hum}}} \qquad 2$$

191 where Δ_i is the change in pool i from day t to $t+1$, B_i is the amount of pool i transformed
192 to biomass from day t to $t+1$, U_i is the amount of pool i transformed to humus from day t to
193 $t+1$, ρ_i is the C:N ratio for pool i, and ρ_{Bio} and ρ_{Hum} are the C:N ratios for the biomass and
194 humus pools respectively. The sum of M_i across the four pools gives the net mineralisation or
195 immobilisation, if the sum of M_i is negative immobilisation occurs and mineral N is removed
196 from the soil, if the sum of M_i is positive mineralisation occurs and mineral N is added as
197 $\mathrm{NH_4^+}$ to the soil. If there is not enough soil mineral N ($\mathrm{NO_3^-}$ and $\mathrm{NH_4^+}$) on a particular day, then

198 decomposition of TOC does not happen. If there is enough soil mineral N, then N is removed
199 from the NH_4^+ pool in preference to NO_3^- pool.

200 The P mineralisation or immobilization of each SOP pool is calculated in a similar way
201 to the mineralisation N, where in Equation (2), ρ_i is the C:P ratio for pool i, and ρ_{Bio} and ρ_{Hum}
202 are the C:P ratios for the biomass and humus pools respectively. When P is mineralised 80%
203 is added to the available P pool, and the remaining 20% is added to the non-available P pool.
204 For P 80% of mineralised P is added to or subtracted from the available P pool, similarly when
205 immobilization of P occurs 80% is taken from the available P pool, and the remaining 20% is
206 taken from the non-available P pool (see section 2.5).

207

208 2.4 *Soil Mineral Nitrogen*

209 In the model, soil mineral N consists of N in ammonium (NH_4^+) and nitrate (NO_3^-).
210 Inputs of N through atmospheric deposition (N_{AtDep}) were set to 35 kg N yr^{-1} (Anon, 1998) for
211 the UK in 1966, decreasing linearly to 20 kg N yr^{-1} in 2012 (pers. comm. Goulding). Like,
212 Sundial (Anon, 1998) it was distributed evenly throughout the year as nitrate. Nitrogen applied
213 as fertilizer enters the NH_4^+ or NO_3^- pools depending on the type of fertilizer applied. When
214 organic amendments are added, N enters the soil inorganic nitrogen pools by mineralisation
215 (see section 2.3).

216 Rainfall runoff mixes in the model with the water and minerals in the top 20 mm of the
217 soil profile. The amount of mineral nitrogen (NH_4^+ and NO_3^-) in runoff from the the top 20 mm
218 of soil (N_{Run}) is given by (Sharpley, 1985)

219 $$N_{\mathrm{Run}} = \frac{N_{\mathrm{Surf}}\, W_{\mathrm{Run}}}{W_{\mathrm{Run}} + W_{\mathrm{Surf}}} \qquad 3$$

where the surface water (W_{Surf}) is given by difference in the volumetric water content at saturation and air dried, multiplied by 20 to give the water (mm) in the top 20 mm, $W_{\mathrm{Run}}$is the water runoff (mm) and the surface N (N_{Surf}) is given by

$$N_{\mathrm{Surf}} = \frac{20}{\delta(1)}\ (N_{NH4} + N_{NO3}) \qquad 4$$

where $\delta(1)$ is the depth of the first layer.

Any nitrate in the soil can potentially move down the soil profile with the water. The concentration of NO_3^- in layer l, ($\gamma_{\mathrm{NO3}}(l)$) is given by:

$$\gamma_{\mathrm{NO3}}(l) = \frac{N_{\mathrm{NO3}}(l)}{W(l)} \qquad 5$$

where $N_{\mathrm{NO3}}(l)$ is the NO_3^- (kg N ha^{-1}) in layer l, $l = 1 \ldots 3$, and $W(l)$ is the water content of layer l.

The amount of NO_3^- (kg N d^{-1}) that moves down each layer l is given by

$$F_{\mathrm{NO3}}(l) = \max(0, \min\{N_{\mathrm{NO3}}(l), \gamma_{\mathrm{NO3}}(l) F_W(l+1)\}) \qquad 6$$

where $F_{\mathrm{W}}(l)$ is the water that flows from layer l to layer $l+1$. The nitrate that moves down from layer 3, $F_{\mathrm{NO3}}(3)$, is N leached out of the profile.

Nitrification is an aerobic process whereby the NH_4^+in the soil is oxidised to form NO_3^- and N_2O. Our models are based on Milne et al. (2005) and Parton et al. (2001). The rate of nitrification depends on the soil properties, such as water filled pore space $\theta/\theta_{\mathrm{Sat}}$, soil temperature (T), soil moisture (M), and pH (S_{pH}). In the model the amount of N_2O (kg N ha^{-1} day^{-1}) produced from a given amount of NH_4^+ ($N_{\mathrm{NH4}}(l)$) in layer l is given by

$$N_{\mathrm{N2O}}(l) = k_{\mathrm{N2O}}\ N_{\mathrm{NH4}}(l) S_{\mathrm{pH}}(l) \left(1 - \frac{\theta}{\theta_{\mathrm{Sat}}(l)}\right), \qquad 7$$

where k_{N2O} is a constant that takes the value 0.0001. The amount of nitrate (kg N ha^{-1} day^{-1}) produced from soil NH_4^+ is given by

$$N_{\mathrm{NO3}}(l) = \max\left[(N_{\mathrm{NH4}}(l) - N_{\mathrm{N2O}}(l) - N_{\min})(1 - e^{-k})\, f\big(T(l)\big) g\big(M(l)\big), 0\right] \quad (8)$$

where $N_{\min}$ is the minimum amount of $\mathrm{NH_4^+}$ that must be in the soil for nitrification to occur (we assume $N_{\min} = 0.05$), k is a constant for nitrification which is set at 0.15, and $f(T)$ and $g\big(M(i)\big)$ are functions that describe the effect respectively of temperature and moisture on nitrification, for details see Godwin and Allan Jones (1991).

Denitrification is an anaerobic process whereby the $\mathrm{NO_3^-}$ in the soil is reduced to nitrous oxide and nitrogen. The amounts of these gases produced depends on the soil conditions, most notably the nitrate in the soil (N_{NO3}, kg ha^{-1}), the water filled pore space ($\theta/\theta_{\mathrm{Sat}}$), soil temperature ($T$, ^{o}C), soil organic carbon (c) and pH (S_{pH}) (Del Grosso et al., 2000; Milne et al., 2011; Nömmik, 1956). The effect of soil organic carbon on emissions is felt indirectly as a result of the temperature function $g(T)$. We assumed the following simple model to describe N_2O emissions (kg N ha^{-1} day^{-1})

$$\mathrm{N_2O} = aN_{\mathrm{NO3}} f(\theta/\theta_{\mathrm{Sat}}) g(T) \quad (9)$$

where a is a constant. We took the functional forms of $f(\theta/\theta_{\mathrm{Sat}})$ and $g(T)$ from the literature and then fitted the model parameters to data from field experiments from around the UK where nitrate, soil temperature, water filled pore space, and N_2O emissions (kg N ha^{-1} day^{-1}) were measured. Similar to other empirical or semi-empirical models, these parameter values can only be assumed to hold for the range of conditions for which they were fitted, and outside of this range further validation would be required. Nitrous oxide is linearly related to nitrate (N_{NO3}) and we used the function defined by Lark and Milne (2016) to describe the effect of water-filled-pore space on N_2O emissions. That is

$$f(w) = \exp\left[-0.6151\left(\log\left\{\frac{\theta/\theta_{\mathrm{Sat}}(l)}{1 - \theta/\theta_{\mathrm{Sat}}(l)}\right\} - 1.19\right)^2\right] \quad (10)$$

where $\theta/\theta_{\mathrm{Sat}}(l)$ is the water filled pore space in each layer l. Data from Nömmik (1956) suggested that the relationship between temperature and N_2O emissions should follow a normal distribution with mean 23.65 and standard deviation 5.53. However, data from the Defra project AC0116 (http://www.environmentdata.org/archive/ghgno:676) which we used to relate average temperature to emissions, did not conform to the standard deviation given by Nömmik (1956). Therefore, we assumed the same mean but fitted the standard deviation to our field data. Our fitted model was

$$\mathrm{N_2O} = 0.000735 N_{\mathrm{NO3}} \exp[-0.6151(\theta/\theta_{\mathrm{Sat}}(l) - 1.19)^2] \exp[-0.00045(T - 23.65)^2] \quad 11$$

which we apply in only the top two layers of our model as there is not sufficient biological activity for denitrification to occur in the bottom soil layer.

When water filled pore space increases, the soil becomes more anaerobic and so the amount of N_2 produced increases. A similar relationship holds for temperature (Nömmik, 1956). We used the following model and fitted the parameters so that our model gave proportions of N_2O to N_2 similar to those observed in Colbourn (1988)

$$\mathrm{N_2} = \frac{0.0052\ \mathrm{N_{NO3}}}{(1 + \mathrm{e}^{-0.14975(T+4.0)})(1 + \mathrm{e}^{-12.0(\theta/\theta_{\mathrm{Sat}}(l)-0.62)})}. \quad 12$$

The nitrogen taken up by the crop each day is taken from the nitrate pool with an upper limit of 6 kg N ha^{-1} day^{-1} (Semenov et al., 2007).

2.5 *Mineral Phosphorus*

In the model, mineral phosphorus is split into two pools: available P (which includes phosphorus in soil solution and loosely adsorbed to the clay surface) and non-available P.

285 Eighty percent of the fertilizer P enters the available P pool and the remaining 20% enters the
286 non-available P pool (Wolf et al., 1987).

287 Similar to the N model, a proportion of the available P contained in the top 20 mm of
288 soil can be lost through runoff.

289 $$P_{\mathrm{Run}} = \frac{P_{\mathrm{Surf}}\, W_{\mathrm{Run}}}{W_{\mathrm{Run}} + W_{\mathrm{Surf}}} \qquad 13$$

290 where the surface P (P_{Surf}) is given by

291 $$P_{\mathrm{Surf}} = \frac{20}{\delta(1)}\, P_{\mathrm{M}} \qquad 14$$

292 where P_{M} is the mobile (dissolved and particulate) P which we assume to be 10% of $P_{\mathrm{AV.}}$We
293 set solution P to 1% of the available P (pers. comm. Paul Poulton). This can potentially be
294 leached when water flows down the profile.

295 The soil organic P that is mineralised is added to the available P pool . Mineral P may
296 also be immobilised, in which case it is taken from the available P pool first and then from the
297 non-available P pool.

298 Available P (P_{Av}) is converted to non-available P (P_{NonAv}) by reversible processes
299 which reduce its extractability. In the model, the P content for each soil layer (available and
300 non-available P), which we define P_{Tot}, is calculated in mg kg^{-1} soil. The release to fixation
301 variable, $V(l)$, for layer l is given by

302 $$V(l) = \begin{cases} \dfrac{\alpha_b\, P_{\mathrm{Tot}}(l) + \beta_b}{P_{\mathrm{Tot}}(l)}, & P_{\mathrm{Tot}}(l) > \dfrac{\beta_a - \beta_b}{\alpha_b - \alpha_a} \\ \dfrac{\alpha_a\, P_{\mathrm{Tot}}(l) + \beta_a}{P_{\mathrm{Tot}}(l)}, & P_{\mathrm{Tot}}(l) \le \dfrac{\beta_a - \beta_b}{\alpha_b - \alpha_a} \end{cases} \qquad 15$$

303

304 were α_b and β_b are the slope and intercept, of value 0.113 and -49.3 respectively, for the
305 linear relationship between P_{Av} and P_{Tot}. For small values of P_{Tot}, an alternative set of

coefficients α_a and β_a, of value 0.0201 and -5.1, are used (see supplementary Fig. 1). The ratio of release to fixation is given by

$$R_{\mathrm{RF}}(l) = \frac{V(l)}{1.0 - V(l)} \quad 16$$

The transfer of P from the non-available to the available pool $P_{\mathrm{NA\rightarrow Av}}$, and the reverse transfer $P_{\mathrm{Av\rightarrow NA}}$ in layer l on day $t + 1$ are given by

$$P_{\mathrm{NA\rightarrow Av}} = R_{\mathrm{RF}}(l)\, P_{\mathrm{Av}}(l;t) f_{\mathrm{pH}}\left(S_{\mathrm{pH}}(l)\right) \quad 17$$

$$P_{\mathrm{Av\rightarrow NA}} = \lambda\, P_{\mathrm{NonAv}}(l;T) R_{\mathrm{RF}}(l) f_{\mathrm{pH}}\left(S_{\mathrm{pH}}(l)\right), \quad 18$$

and so

$$P_{\mathrm{NonAv}}(l;t+1) = P_{\mathrm{NonAv}}(l;t) + P_{\mathrm{Av\rightarrow NA}} - P_{\mathrm{NA\rightarrow Av}} \quad 19$$

$$P_{\mathrm{Av}}(l;t+1) = P_{\mathrm{Av}}(l;t) - P_{\mathrm{Av\rightarrow NA}} + P_{\mathrm{NA\rightarrow Av}} \quad 20$$

The constant λ determines the rate of re-equilibration between P_{Av} and P_{NonAv} following the addition of mineral P, and is set to 0.01 giving a half-life of approximately 65 days. The values of coefficients, α, β and λ were established for a silty clay loam soil at Rothamsted. The rate modifying function f_{pH} linearly increases from 0.0 to 1.0 as pH increases from 0 to 7, and then linearly decreases back to zero as pH increases from 7 to 14. The P required by the crop is taken from the available P pool, up to a limit of 2 kg P ha^{-1} day^{-1}.

2.6 Bulk density

To take into account changes in depth caused by changes in bulk density as a result of, for example, the addition of FYM, we used the Rawls (1983) nomogram to estimate bulk density in relation to sand, clay and organic carbon contents of soil. The depth of the topsoil is

modified to reflect the change in bulk density (changes in depth and bulk density only occur in the top soil). Because of the changes in depth and bulk density in the top soil, we modify water properties, such as the water content at saturation, field capacity, and wilting point, daily (see section 2.2). Modelling bulk density dynamically in this way has been described previously by Whitmore et al. (2011).

2.7 Crop model

Our crop model is a generic plant growth model, which uses a light use efficiency (LUE, g dry matter MJ^{-1}) based approach to calculate the biomass production (Monteith, 1990; Monteith and Moss, 1977). The rate of biomass (B_{crop}) produced each day is given by

$$\frac{dB_{\mathrm{crop}}}{dt} = Q\ \varepsilon\ W_{\mathrm{rf}}\ N_{\mathrm{NI}}\ P_{\mathrm{NI}} \qquad 21$$

where Q is the intercepted PAR (MJ PAR m^{-2} surface area) which depends on the solar radiation and canopy leaf area, ε is the crop specific LUE, which for grass, changes with development stage see Schapendonk et al. (1998), W_{rf} is the transpiration reduction factor, N_{NI} and P_{NI} are the nitrogen and phosphorus nutrition indices, which range from zero to one. For grass, LUE is reduced for higher radiation levels (Schapendonk et al., 1998). In our model LUE is reduced by a factor R_{LUE} which decreases from 1.0 to 0.33 when radiation increases from 10 to 40 MJ m^{-2} d^{-1}. Schapendonk et al. (1998) also modified LUE, by the temperature factor T_{LUE}, which in this study increases linearly from 0.0 to 1 between 6.0 and 9.0 ^{o}C. The biomass formed is partitioned between roots, stem, leaves and storage organs based on the development stage (DVS) (Boons-Prins et al., 1993; Wolf, 2012).

The transpiration reduction factor (W_{rf}) is defined as the ratio of actual transpiration (mm day^{-1}) to potential transpiration (mm day^{-1}) and is calculated

$$W_{\mathrm{rf}} = \frac{\sum_{l=1}^{3} A_{\mathrm{Tran}}(l)}{P_{\mathrm{Tran}}} \qquad 22$$

where P_{Tran} is the daily potential transpiration which is calculated as in Lintel (Wolf, 2012). The amount of the actual transpiration coming out of layer (l) is given by

$$A_{\mathrm{Tran}}(l) = \frac{P_{\mathrm{Tran}}(l) W_S(l)^2 \, F_{\mathrm{RL}}(l)}{W_S(1)\, F_{\mathrm{RL}}(1) + W_S(2)\, F_{\mathrm{RL}}(2) + W_S(3)\, F_{\mathrm{RL}}(3)}. \qquad 23$$

Here F_{RL} is the fraction of root in each layer and W_S is the impact of water content on the water stress function. This follows the approach of Li et al. (2001). This impact of water content is based on the method described in Feddes et al. (1976) given by

$$W_S = \begin{cases} \dfrac{\theta_s - \theta}{\theta_s - \theta_a}, & \text{for} \quad \theta > \theta_a \\ 1 & \text{for} \quad \theta_a \geq \theta > \theta_d \\ \dfrac{\theta - \theta_w}{\theta_d - \theta_w}, & \text{for} \quad \theta_d \geq \theta > \theta_w \end{cases} \qquad 24$$

where θ is the volumetric water content, θ_s is the water content at saturation, θ_a is the water content at -5 kPa, θ_d is the water content at -40 kPa, and θ_w is the water content at wilting point (-1500 kPa). Water stress affects grass less than arable crops (per comms J. Storkey). In simulations, when the soil is saturated grass does not suffer water stress. When the volumetric water content falls below $\theta_d = -40$ kPa the water stress factor W_S decreases linearly between θ_d and θ_w to 0.4.

The proportion of root (F_{RL}) in each layer l is given by

$$F_{RL}(l) = \frac{R_{\mathrm{Len}}(l)}{R_{\mathrm{Len}}(1) + R_{\mathrm{Len}}(2) + R_{\mathrm{Len}}(3)} \qquad 25$$

where R_{Len} is the root length per unit area (mm mm^{-2}).

The root depth (d_{root}) increases by 12.0 mm per day to a maximum root depth which depends on the crop being modelled. The root length per unit area within each layer, calculated according to an adaptation of the method of Gerwitz and Page (1974), is given by

$$R_{\mathrm{Len}}(l) = -\frac{R_0}{a\,(e^{-a\,Z_2(l)} - e^{-a\,Z_1(l)})} \quad 26$$

where R_0 is the root length density at the soil surface (mm mm^{-3}) the value of which is non-essential to the model as it cancels out in Equation (25), $z_1(l)$ and $z_2(l)$ are the upper and lower horizon depth (mm) of layer l, and a is given by

$$a = -\frac{\ln(1 - F_{\mathrm{r}})}{d_{\mathrm{root}}} \quad 27$$

where F_{r} is the fraction (arbitrarily defined as 0.98) of the root length that is present above d_{root}.

The uptake of plant nutrient (N and P) is determined by the crop demand and the supply of these nutrients by soil. The total nutrient demand of the crop is the sum of the nutrient demand from its individual organs (i.e. roots, stems and leaves excluding storage organs, for which nutrient demand is met by translocation from the other organs). Nutrient demand of the individual organs is calculated as the difference between maximum and actual organ nutrient contents. The maximum nutrient content is defined as a function of canopy development stage. The total nutrient uptake of the crop takes place before anthesis. Sub-optimal nutrient availability in the soil leads to nutrient stress in the crop. A detailed description of crop nitrogen dynamics is reported by Shibu et al. (2010) and P dynamics follows N in a similar way.

Nitrogen stress in the plant growth model is expressed as nitrogen nutrition index (N_{NI}) and is calculated by:

$$N_{\mathrm{NI}} = \max\left[0, \min\left(1, \frac{N_{\mathrm{leaf}} + N_{\mathrm{stem}} - N_{\mathrm{Res}}(\Omega_{\mathrm{leaf}} + \Omega_{\mathrm{stem}})}{\Omega_{\mathrm{leaf}} N_{\mathrm{MaxPropleaf}} + \Omega_{\mathrm{stem}} N_{\mathrm{MaxPropstem}} - N_{\mathrm{Res}}(\Omega_{\mathrm{leaf}} + \Omega_{\mathrm{stem}})}\right)\right] \quad 28$$

where N_{leaf} and N_{stem} are the N in the leaf and stem respectively, Ω_{leaf} and Ω_{stem} are the weights of the leaf and stem respectively, $N_{\mathrm{MaxPropleaf}}$ and $N_{\mathrm{MaxPropstem}}$ are the maximum proportion of N in the leaf and stem respectively. The residual N (N_{Res}) is the fraction of N

which is part of the cell structure and was fixed at 0.004 for wheat (Wolf, 2012) and 0.01 for grass (Bouman et al., 1996). For wheat, the maximum N in the leaf is given by:

$$N_{\mathrm{MaxPropleaf}} = 0.046\exp(-1.7D) + 0.014 \quad (29)$$

where D is the development stage of the crop which is calculated using thermal time modified by a vernalisation factor and the photosensitivity of the crop (see Wolf (2012), and references therein). For grass we set $N_{\mathrm{MaxPropleaf}}$ to 0.0425. The maximum N in the stem is given by $N_{\mathrm{MaxPropStem}} = 0.5\, N_{\mathrm{MaxPropLeaf}}$, (see Wolf (2012).

The phosphorus nutrition index (P_{NI}) is calculated by:

$$P_{\mathrm{NI}} = \max\left[0, \min\left(1, \frac{P_{\mathrm{leaf}} + P_{\mathrm{stem}} - (\Omega_{\mathrm{leaf}}\, P_{\mathrm{ResLeaf}} + \Omega_{\mathrm{stem}} P_{\mathrm{ResStem}})}{\Omega_{\mathrm{leaf}} P_{\mathrm{MaxPropleaf}} + \Omega_{\mathrm{stem}} P_{\mathrm{MaxPropstem}} - N_{\mathrm{Res}}(\Omega_{\mathrm{leaf}}\, P_{\mathrm{ResLeaf}} + \Omega_{\mathrm{stem}} P_{\mathrm{ResStem}})}\right)\right] \quad (30)$$

where P_{leaf} and P_{Stem} are the P in the leaf and stem respectively, and $P_{\mathrm{MaxPropleaf}}$ and $P_{\mathrm{MaxPropstem}}$ are the maximum proportion of P in the leaf and stem respectively. For wheat the residual P in the leaf is $P_{\mathrm{ResLeaf}} = 0.0003$ and in the stem $P_{\mathrm{ResStem}} = 0.00018$. For grass both P_{ResLeaf} and P_{ResStem} are set to 0.001 (Wolf et al., 1987). For wheat the maximum P in the leaf reduces with development stage. From development stages 0 to 0.7 it reduces linearly from 0.0066 to 0.0036 and then from 0.0036 to 0.0009 from development stage 0.7 to 1, after which it holds the value of 0.0009. For grass the maximum P in the leaf is fixed at 0.0035 (Bouman et al., 1996).

Processes leading to the aboveground litter formation and carbon turnover below ground are similar for both crops and grass but their rates are different. We assume that 50% of the dead leaves become litter on a daily basis and the remainder is left on the stem. The rate at which the roots die is a function of growth stage. In case of crops, the root death happens towards the latter part of the growing season (DVS >1.5) at a rate of 0.02 per day. In case of

grass, once the root system has been established (3-6 months after sowing, DVS=0.01), root death becomes continuous at a rate of 0.01 per day. The root exudates are considered to be a part of root death, so are not modelled seperately . The leaf death rate is a function of heat stress, nitrogen stress and shading as described in Schapendonk et al. (1998). All C, N, and P from dead roots and litter is returned to the soil.

The grass model differs somewhat from the crop model as grass has indeterminate growth and is not allowed to flower (so always has a DVS always < 1.0) as it can be cut or grazed in the model (unlike the crop which completes its life cycle in a given growing season). Grass is a perennial crop that grows for one or more seasons before being reseeded. Cut grass and grazed grass is removed from the modelled system. The amount removed is such that the remaining biomass cannot fall bellow 50 g m^{-2}. Livestock deposit nutrients into the system as manure. When animals are on the field, we set the deposition of C and N for each animal type based on data from (Cottrill and Smith, 2007), for each beef animal this was 4.03 kg C of manure per day containing 0.22 kg N, for each dairy cow this was 6.45 kg C per day containing 0.35 kg N, and for each sheep this was 0.45 kg C per day as fresh deposit, containing 0.02 kg N per day. These rates are multiplied by the stocking rate to give the rate of deposit per hectare.

2.8 *Data requirements*

For each layer of the soil, the model requires initial values for soil depth, clay, silt, TOC, bulk density, available P, non available P, soil NH_4, soil NO_3, soil pH. Initial values for elevation and latitude are also needed. The model runs with a daily time-step and so for each simulated day weather data (minimum and maximum temperature, rainfall, radiation, vapour pressure and windspeed) are needed. For each season and where relevant to the crop, sowing dates, fertilizer application timing, type and dose and dates when the grass is cut are required.

441 *2.9 Case studies*

442 To test our model, we used data from two long-term agricultural experiments and one
443 more recent grass-livestock experiment. These were: The Broadbalk wheat experiment, and
444 the Park Grass permanent grassland experiment at Rothamsted Research, Hertfordshire, UK
445 (51.8° N, 0.37 ° W), and the more recent North Wyke farm platform at Rothamsted Research,
446 near Okehampton, UK (50.77° N, 3.92 ° W), which has spatially integrated data from livestock-
447 bearing grassland in a sloping terrain. We used a suite of statistical metrics (including the mean,
448 standard deviation, root mean square error, and sample correlation coefficient, r) to quantify
449 the performance of our model (see Smith et al., 1997).

450

451 2.9.1 *Broadbalk*

452 The Broadbalk wheat experiment has been running since 1843, and wheat has been
453 sown and harvested on all or part of the experiment every year since then. The original aim of
454 the experiment was to test the effects of various combinations of inorganic fertilizers and
455 organic manures on the yield of winter wheat. The experiment was divided into different strips
456 given a range of fertilizer applications, which extended the whole length of the field. In 1926
457 the experiment was divided into five Sections, crossing the fertilizer treatments at right angles,
458 where each section was bare fallowed one year in five to control weeds. In 1968 the experiment
459 was further divided into 10 Sections, so that the yield of wheat grown continuously could be
460 compared with that grown in rotation after a two-year break. The plots receive management
461 consistent with standard practice for the time. The soil is clay loam to silty clay loam,
462 predominately Batcombe series (Avery and Catt, 1995), FAO classification: Chromic Luvisol
463 (or Alisol), U.S. Soil Taxonomy: Aquic (or Typic) Paleudalf. The site is thought to have been

in arable cropping for many centuries before the start of the experiment. Further details are available from http://www.era.rothamsted.ac.uk/Broadbalk

The plots from the continuous wheat sections (Section 1 and 9), selected for this study, receive a range of fertilizer and FYM applications (see Table 1). Wheat has been grown every year on these Sections, since 1966. Modern, short-strawed high yielding varieties were introduced in the 1967–1968 season and it is from this date that we test the model. Most of the data are available from the electronic Rothamsted Archive (eRA http://www.era.rothamsted.ac.uk). Periodic measurements of TOC were made on all plots (Watts et al., 2006; Pers. comm. P. Poulton for later data), measurements of volumetric water content on plot 8 in 2007 (Pers. Comm, C. Watts) and measurements and estimates of N leaching were made between 1990 and 1998 (Goulding et al., 2000). Grain N was measured 1968-2012, and grain P from 1968-2011 (except 1976-1985), Section 1 only.

Table 1. The fertilizer and manure treatments applied annually to the Broadbalk experiment plots used in the simulations.

	Treatments				
Plot	up to 1967	1968 - 1984	1985 - 2000	2001 - 2004	2005 - 2012
3	Nil	Nil	Nil	Nil	Nil
5	P K Na Mg	P K Na Mg	P K Mg	K Mg	K Mg
6	48N P K Na Mg	48N P K Na Mg	48N P K Mg	48N K Mg	48N K Mg
7	96N P K Na Mg	96N P K Na Mg	96N P K Mg	96N K Mg	96N K Mg
8	144N P K Na Mg	144N P K Na Mg	144N P K Mg	144N K Mg	144N K Mg
9	48N* P K Na Mg	192N P K Na Mg	192N P K Mg	192N K Mg	192N K Mg
15	96N P K Na Mg	192N P K Na Mg	240N P K Mg	240N K Mg	240N K Mg
16	96N* P K Na Mg	96N P K Na Mg	288N P K Mg	288N K Mg	288N K Mg

2.1	FYM since 1885	FYM 96N	FYM 96N	FYM 96N	FYM 144N
2.2	FYM	FYM	FYM	FYM	FYM

The values of N are in kg N ha^{-1}, applied as ammonium sulphate 1843-1967, as calcium ammonium nitrate between 1968-1985, and as ammonium nitrate thereafter. Treatments with * were applied as sodium nitrate. Farmyard manure (FYM) was applied at 35 t ha^{-1} fresh weight, and contains approximately 250kg N ha^{-1}. Other elements were applied at 35 kg P ha^{-1}, 90 kg K ha^{-1}, 16 kg Na ha^{-1} until 1973 and 12 kg Mg ha^{-1} respectively. P has not been applied since 2001, due to high levels of plant available P in the soil. For more details see http://www.era.rothamsted.ac.uk/Broadbalk

We ran the model to simulate the plots listed in Table 1 using weather data from the Rothamsted meteorological station from 1966 to 2012. Comparisons were made between measured and simulated values of crop yield, content of N and P in the grain, TOC, volumetric water content and nitrate leaching.

2.9.2 *Park Grass*

The Park Grass experiment is the oldest experiment on permanent grassland in the world. Started by Lawes and Gilbert in 1856, its original purpose was to investigate ways of improving the yield of hay by the application of inorganic fertilizers and organic manure. Within 3 years it became clear that these treatments were having a dramatic effect on the species composition of what had been a uniform sward. The continuing effects of the original treatments on species diversity and on soil function, together with later tests of liming and interactions with atmospheric inputs and climate change (Storkey et al., 2015), has meant that Park Grass has become increasingly important to ecologists, environmentalists and soil

scientists. The soil is silty clay loam, predominately Hook series, with areas more typical of the Batcombe series (Avery and Catt, 1995), FAO Classification: Chromic Luvisol (or Alisol), U.S. Soil Taxonomy: Aquic (or Typic) Paleudalf. The site is known to have been in permanent pasture for at least 100 years before the start of the experiment. For further details see http://www.era.rothamsted.ac.uk/Park

The plots are cut in mid-June, and made into hay. A second cut is usually taken in the autumn, except in a few years, when there was insufficient herbage to sample. Since 1960, yields have been estimated from strips cut with a forage harvester. The remainder of the plot is still mown and made into hay, continuing earlier management. For the second cut, the whole of each plot is cut with a forage harvester. The experiment is never cultivated, and the site was in permanent grassland for at least 100 years before the experiment began. Further details are available from http://www.era.rothamsted.ac.uk/Park

Here we simulated two plots, Plot 3a and 14/2a, with contrasting fertilizer treatments. Plot 3a has received no inorganic fertilizer or manure since 1856. Plot 14/2a has received 96 kg N ha^{-1} in the spring, and 35 kg P in the autumn each year since 1858, plus K, Na and Mg. In 1965 the plots were divided into four subplots, given different amounts of chalk to maintain soil at pHs of 7, 6 and 5 (sub-plots a, b and c, respectively). The fourth sub plot (d) receives no chalk. We have selected sub-plot 'a' for this simulation, with a pH of 7. We use yield data from 1966-2012, with two cuts each year except in 2003, when no second cut was taken, with weather data from the Rothamsted meteorological station.

We chose Plot 14/2a over the other N fertilizer plots because N is applied as sodium nitrate, whereas in most other plots N is applied as ammonium sulphate, which has an acidifying effect on the soil and so a dramatic effect on species composition and the decomposition of soil organic matter (see http://www.era.rothamsted.ac.uk/Park).

524

525 2.9.3 *The North Wyke Farm Platform*

526 The North Wyke Farm Platform, near Okehampton, SW England was established as a UK
527 National Capability for collaborative research, training and knowledge exchange in agro-
528 environmental sciences related to beef and sheep production in lowland grasslands (Orr et al.,
529 2016). The soils on the farm platform are predominately Halstow, (Pelo-stagnogley soils,
530 Avery, 1980), FAO Classification: Stagni-vertic cambisol, U.S. Soil Taxonomy: Typic
531 haplaquept. For more details see Harrod and Hogan (2008). A system based on permanent
532 pasture was implemented on three 21-ha farmlets to obtain baseline data on hydrology, nutrient
533 cycling and productivity for 2 years. Since then, two of the farmlets have been modified by
534 either (i) planned reseeding with grasses that have been bred for enhanced sugar content or
535 deep-rooting traits or (ii) sowing grass and legume mixtures to reduce nitrogen fertilizer inputs.
536 The third farmlet continued under permanent pasture. The quantities of nutrients that enter,
537 cycle within and leave the farmlets are recorded using sensor technologies alongside more
538 traditional field study methods. Here we simulated the water and nutrient flows from October
539 2012 to 25th December 2013 from catchment 4 (Golden Rove) and catchment 5 (Orchard
540 Dean), two of the un-modified permanent grassland catchments, that had contrasting
541 topologies. The North Wyke data that we used for this study are available from
542 http://www.rothamsted.ac.uk/farmplatform).

543

544 2.10 *Trade offs*

545 We coupled the simulation model with an optimisation algorithm to determine Pareto
546 optimal fronts between multiple objectives defined in terms of outputs from the model. The
547 optimised Pareto fronts describe the trade-offs between objective variables such as yield and

548 nitrate leaching. To illustrate how these can be identified, we used the fertiliser application
549 time and amount as two management variables that the optimisation algorithm could vary in
550 order to affect three objectives: the yield of a wheat crop, nitrate leaching and N_2O emissions.
551 Simulations used the soil properties and weather data from plot 9 of the Broadbalk experiment
552 for the years 1968–1978. For this period the mean measured yield was 5.4 t ha^{-1} at 85% dry
553 matter.

554 Initially the algorithm, which combines non-dominated sorting (Deb et al., 2002) with
555 differential evolution (Storn and Price, 1997), randomly selects a number of possible
556 management variables, implements these management options in the simulation model and
557 records the effect on each of the multiple objectives. Non-dominated sorting then identifies the
558 management options that result in the 'best' objectives, i.e. those that are non-dominated. A
559 point is said to be dominated by another if it is worse for every single objective. For example,
560 if we aim to maximise two objectives, point A (Fig. 2) is dominated by point B because the
561 value of both objectives is greater at B than A. Points B and C, however, are both non-
562 dominated with respect to one another because whilst objective 1 is higher for B, objective 2
563 is higher for C. The non-dominated sorting algorithm performs a series of pairwise
564 comparisons in order to identify all of the management options that lead to non-dominated sets
565 of objectives. The differential evolution algorithm then combines aspects of the management
566 options that led to non-dominated objectives to identify new management options that could
567 potentially perform even better. The process is iterated in directions that the differential
568 evolution algorithm suggests will be an improvement, , until the results converge and produce
569 a similar Pareto front with each iteration.

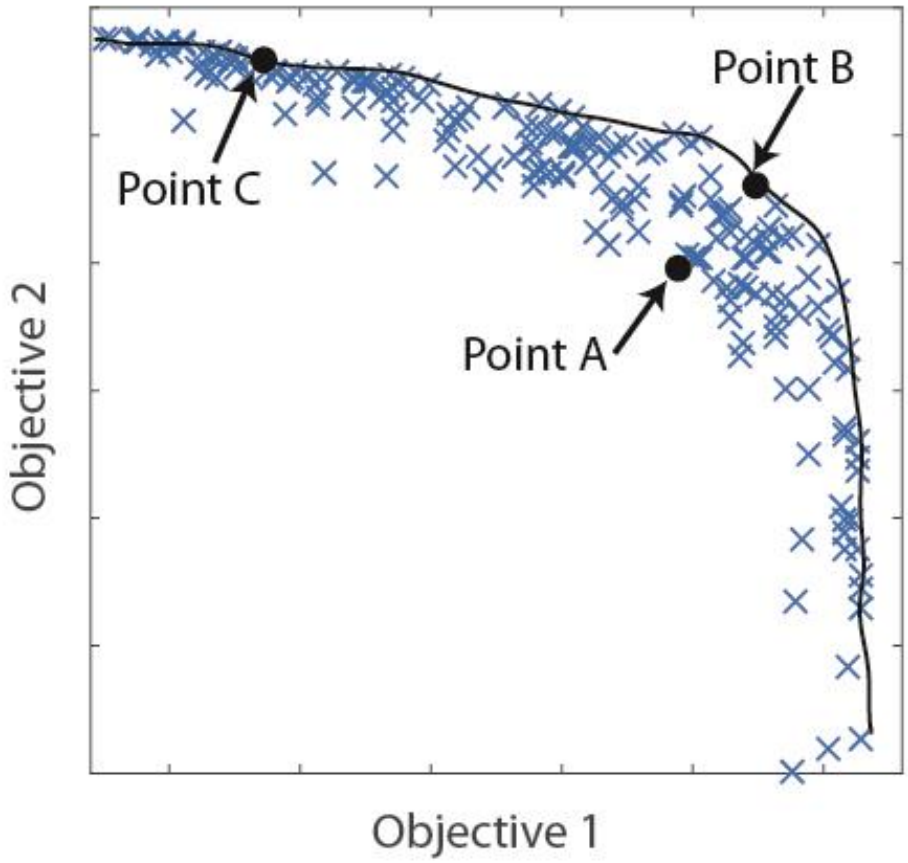

570

571 Fig.2 Example of how a Pareto front is identified from a number of points simulated by the
572 model with the aim to improve multiple objectives (1 & 2) simultaneously. Point B is selected
573 over point A because B scores better for both objectives. It can be seen that neither of points B
574 or C dominates the other, because point B does better at objective 1 whilst point C improves
575 on objective 2. Consequently, both are retained. The Pareto front (line) can be identified by
576 connecting together all of the non-dominated points.

577

578 **3. Results**

579 *3.1 Broadbalk*

580 The simulated and measured grain yields for the plots listed in Table 1 are shown in
581 Fig. 3. The model captures the differences between the plots well and this is quantified by the

582 overall correlation between modelled and measured (Pearson correlation, $r = 0.86$). The plot
583 means for the modelled and measured yields are similar, as are the variances, although the
584 variance for the modelled yield in plots with little fertilizer N applied are smaller than the
585 observed (Table 2). The model reflects the year-to-year fluctuations in yield, although notably
586 under-predicts the 1995 yield from the plots with larger N applications (9, 15, 16, 2.1 and 2.2).

587

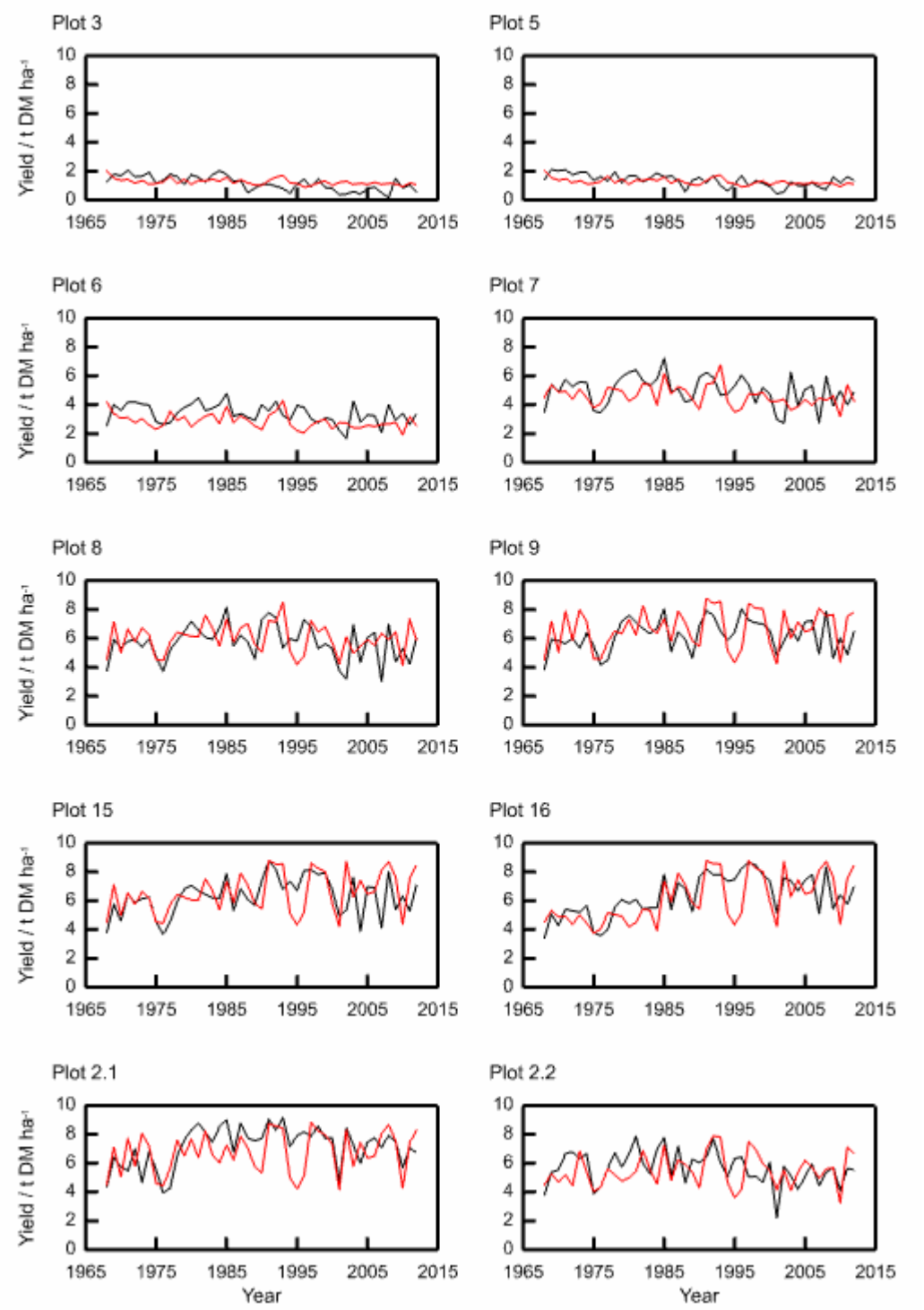

588

589 Fig. 3 Measured (black) and modelled (red) grain yields for ten plots from the Broadbalk

590 long-term wheat experiment, 1968-2012, continuous wheat (sections 1 and 9). The measured

591 values were averaged over Sections 1 and 9 (see 2.9.1).

592

593 The model replicates the plot-to-plot and year-to-year variation in grain N, grain P and
594 TOC (see Figs 4, 3 and 6, and Tables 3, 4 and 5), although we note that year-to-year variation
595 in TOC is minimal. The correlations across all plots between modelled and measured grain N,
596 grain P, and TOC are 0.88, 0.84 and 0.99 respectively. The model reproduces the pattern in the
597 variation of volumetric water content for plot 8, following one of the observed realisations
598 closely (Fig. 7). Note that measurements with such probes are sometimes biased towards drier
599 measurements because instrument range is short and if contact is lost between the access tube
600 and soil then the soil can appear drier than it actually is.

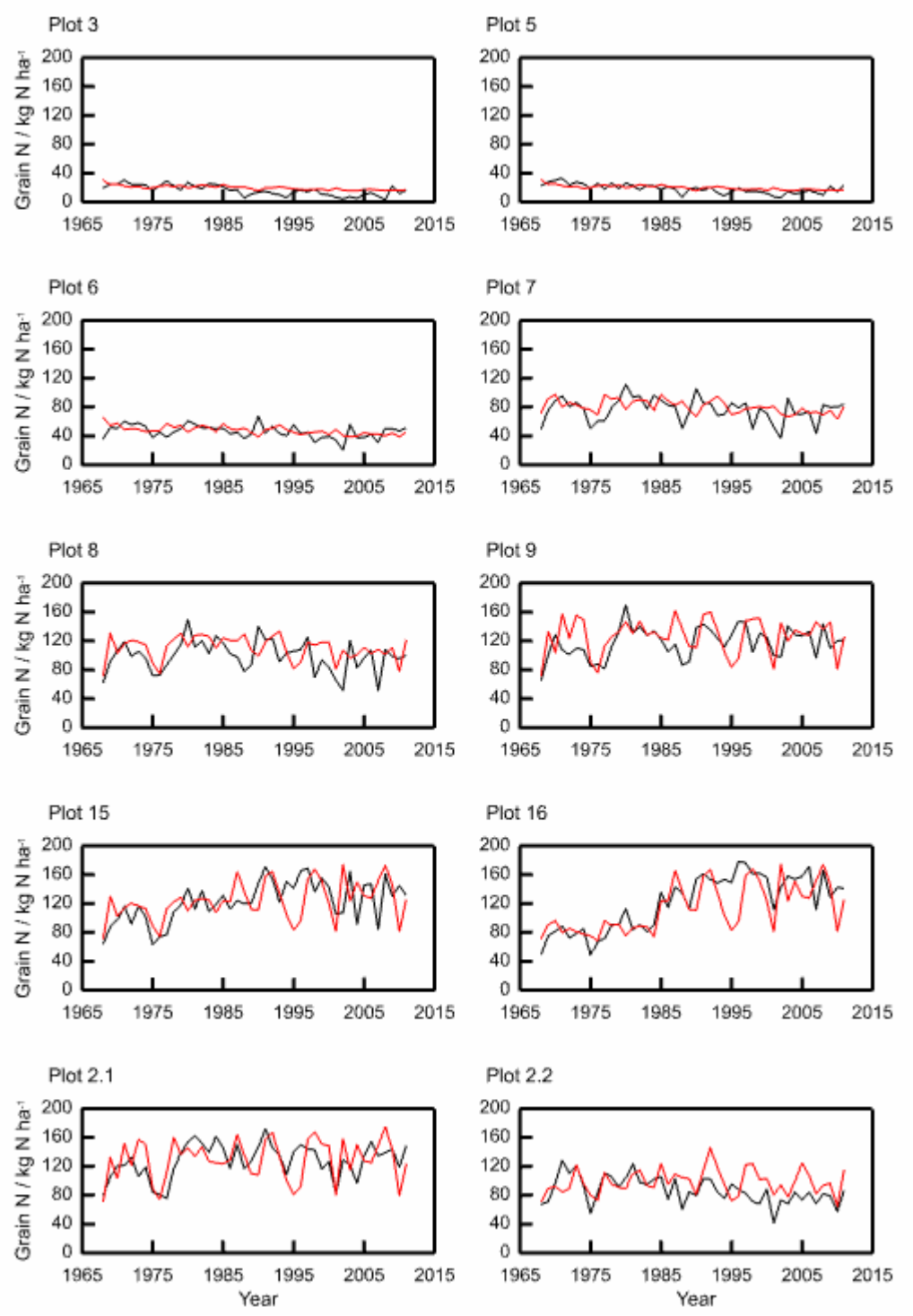

601

602 Fig. 4: Measured (black) and modelled (red) grain N content for ten plots from the Broadbalk
603 long-term wheat experiment, 1968-2012, continuous wheat. The measured values were from
604 Section 1 only (see 2.9.1).

605

606

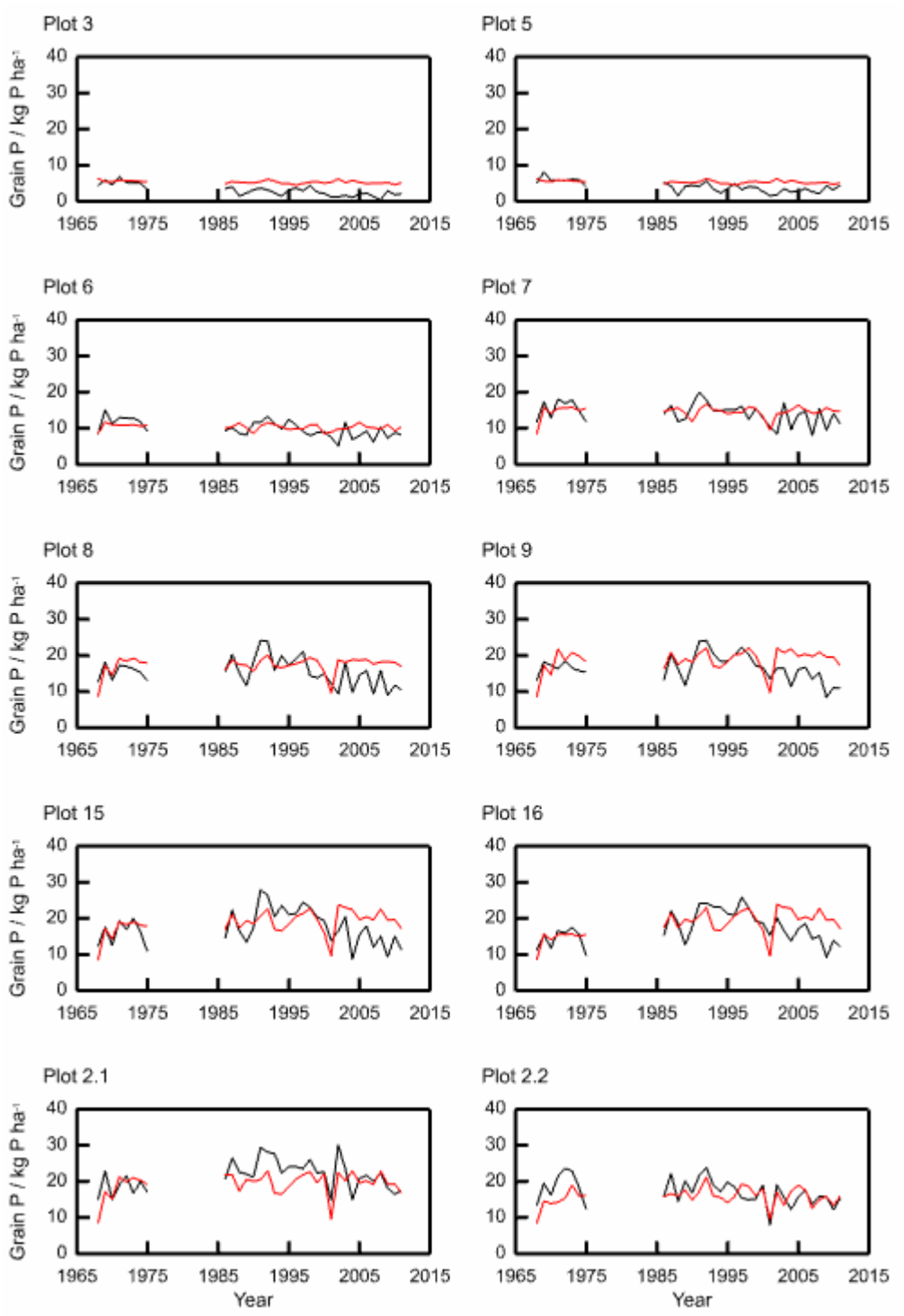

607

608 Fig. 5: Measured (black) and modelled (red) grain P content for ten plots from the Broadbalk

609 long-term wheat experiment (1968–1975 and 1986–2011), continuous wheat. The measured

610 values were from Section 1 only (see 2.9.1)

611

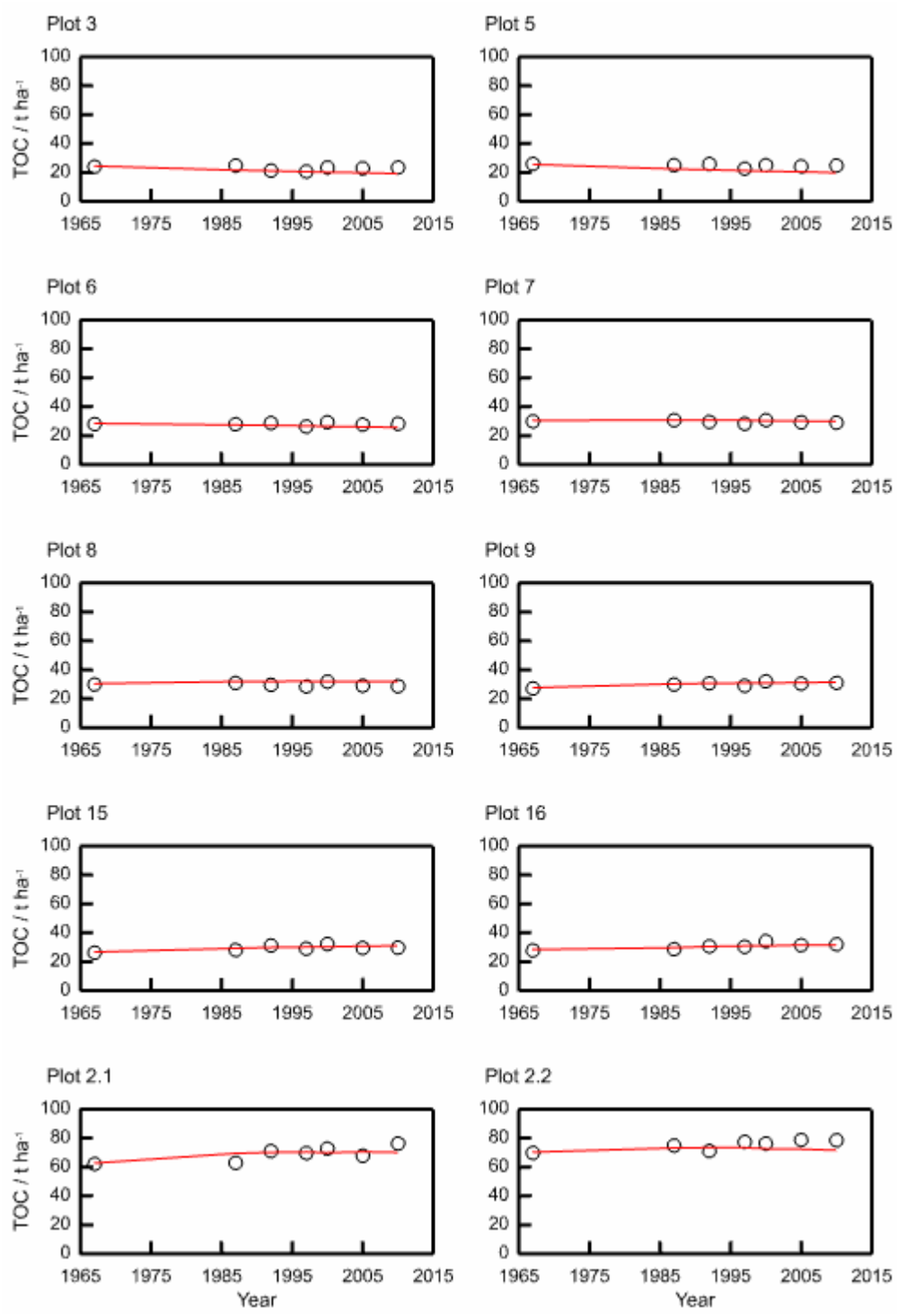

612

613 Fig. 6: Measured (black circles) and modelled (red) soil total organic carbon (TOC) for ten
614 plots from the Broadbalk long-term wheat experiment. The measured values were averaged
615 over Sections 1 and 9.

616

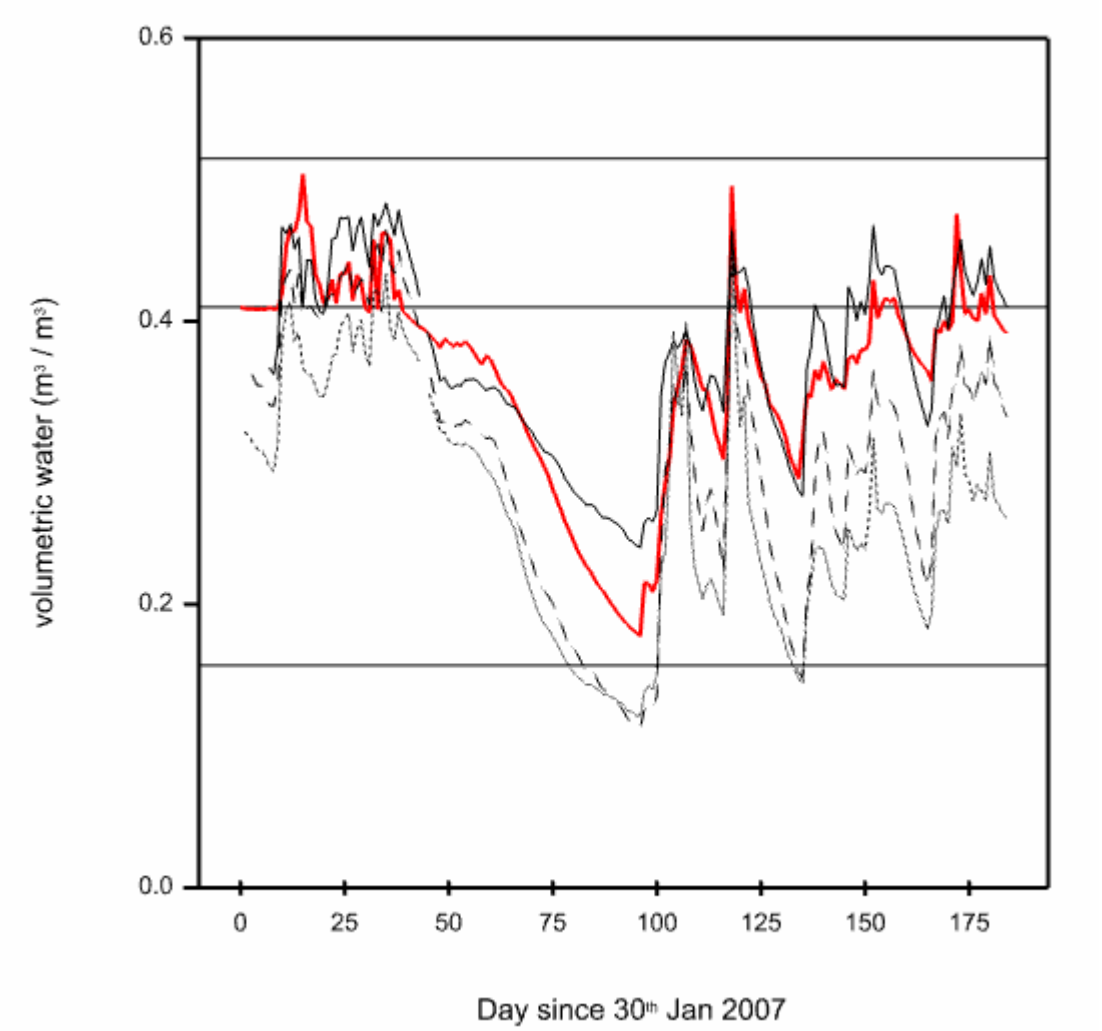

617

618 Fig. 7: Measured for three replicates (black) and modelled (red) volumetric water content in

619 soil from plot 8 of the Broadbalk experiment.

620

621

622 Table 2 Summary statistics for measured and simulated grain yields (at 85% dry matter),
623 19682012 for the Broadbalk wheat experiment. The measured values for yield in each year
624 were averaged over Sections 1 and 9 (see 2.9.1).

	Measured		**Simulated**			
Plot no.	Mean t ha^{-1}	Standard deviation/ t ha^{-1}	Mean t ha^{-1}	Standard deviation/ t ha^{-1}	RMSE (%)	Correlation
3	1.16	0.5	1.26	0.22	42.56	0.28
5	1.37	0.42	1.27	0.22	33.41	0.16
6	3.4	0.67	2.86	0.51	28.61	0.07
7	4.99	1.02	4.62	0.7	24.03	0.16
8	5.71	1.18	6	1.01	24.27	0.25
9	6.23	1.06	6.66	1.32	23.01	0.36
15	6.32	1.28	6.58	1.37	23.29	0.4
16	6.34	1.41	6.12	1.64	20.88	0.64
2.1	7.16	1.35	6.75	1.41	20.28	0.49
2.2	5.67	1.12	5.49	1.13	22.84	0.35

625
626

627 Table 3 Summary statistics for measured and simulated grain N content, 1968–2012, for the
628 Broadbalk wheat experiment. The measured values for grain N were from Section 1 only (see
629 2.9.1).

630

	Measured		**Simulated**			
Plot no.	Mean kg N ha^{-1}	Standard deviation/ kg N ha^{-1}	Mean kg N ha^{-1}	Standard deviation/ kg N ha^{-1}	RMSE (%)	Correlation
3	16.33	7.23	19.76	3.1	42.54	0.57
5	18.48	6.36	20.07	3.15	31.58	0.47
6	46	9.12	47.69	5.79	23.42	0.03
7	76.69	16.21	80.44	9.03	23.58	0.11
8	99.03	21.31	110.25	15.84	25.44	0.29
9	117.91	20.91	126.27	23.92	23.32	0.32
15	122.99	28.03	124.05	25.96	25.17	0.35
16	121.34	37.12	113.62	32.82	22.98	0.71
2.1	128.08	23.56	129.28	27.52	21.27	0.44
2.2	86.83	18.58	98.09	17.27	27.04	0.34

631

632

633 Table 4 Summary statistics for measured and simulated P in the grain, 1968–1975 and 1986–
634 2011 for the Broadbalk wheat experiment. The measured values for grain P were from
635 Section 1 only (see 2.9.1).

636

	Measured		**Simulated**			
Plot no.	Mean kg P ha^{-1}	Standard deviation/ kg P ha^{-1}	Mean kg P ha^{-1}	Standard deviation/ kg P ha^{-1}	RMSE (%)	Correlation
3	3.04	1.49	5.36	0.43	89.47	0.29
5	4.05	1.47	5.4	0.43	48.33	0.26
6	9.89	2.23	10.35	0.86	22.5	0.26
7	14.11	2.89	14.58	1.66	20.73	0.29
8	15.38	3.85	17.31	2.38	29.01	0.23
9	16.49	3.59	18.64	3.06	27.8	0.26
15	17.47	4.73	18.77	3.27	28.34	0.33
16	17.33	4.3	18.42	3.57	25.47	0.42
2.1	21.49	4.09	19.36	3.26	20.42	0.47
2.2	17.14	3.57	15.8	2.5	20.24	0.49

637

638

639 Table 5 Summary statistics for measured and simulated total soil organic carbon (TOC),
640 when measured between 1967–2012 Broadbalk wheat experiment. The measured values for
641 TOC were averaged over Sections 1 and 9 (see 2.9.1).

642

	Measured		**Simulated**			
Plot no.	Mean t C ha^{-1}	Standard deviation/ t C ha^{-1}	Mean t C ha^{-1}	Standard deviation/ t C ha^{-1}	RMSE (%)	Correlation
3	22.95	1.37	21.01	1.6	11.51	0.28
5	24.84	1.05	21.78	1.76	13.83	0.47
6	27.96	0.88	26.82	0.84	6.07	-0.08
7	29.57	0.83	30.39	0.3	3.88	0.24
8	29.73	1.12	31.69	0.53	7.88	-0.1
9	29.97	1.47	30.36	1.18	3.11	0.82
15	29.45	1.84	29.74	1.33	4.42	0.72
16	30.75	1.96	30.55	1.06	4.3	0.78
2.1	68.9	4.76	68.97	2.61	5.46	0.62
2.2	75.18	3.27	72.36	1.06	5.61	0.28

643

644

645 The measured (Goulding et al., 2000) and modelled N leached for each plots are shown
646 in Fig. 8. The model predictions match the N leached from the mineral fertilized plots
647 reasonably well, although the model consistently overestimates N leached from plots receiving
648 the most N (plots 15 and 16 and the FYM plots 2.1 and 2.2) and in the driest years (1991/2,
649 1996/7 and 1997/8). The variances for measured leaching are larger than the modelled for all
650 but plot 2.1 (Table 6). Note that measurements were not determined for every plot in every
651 year.

652

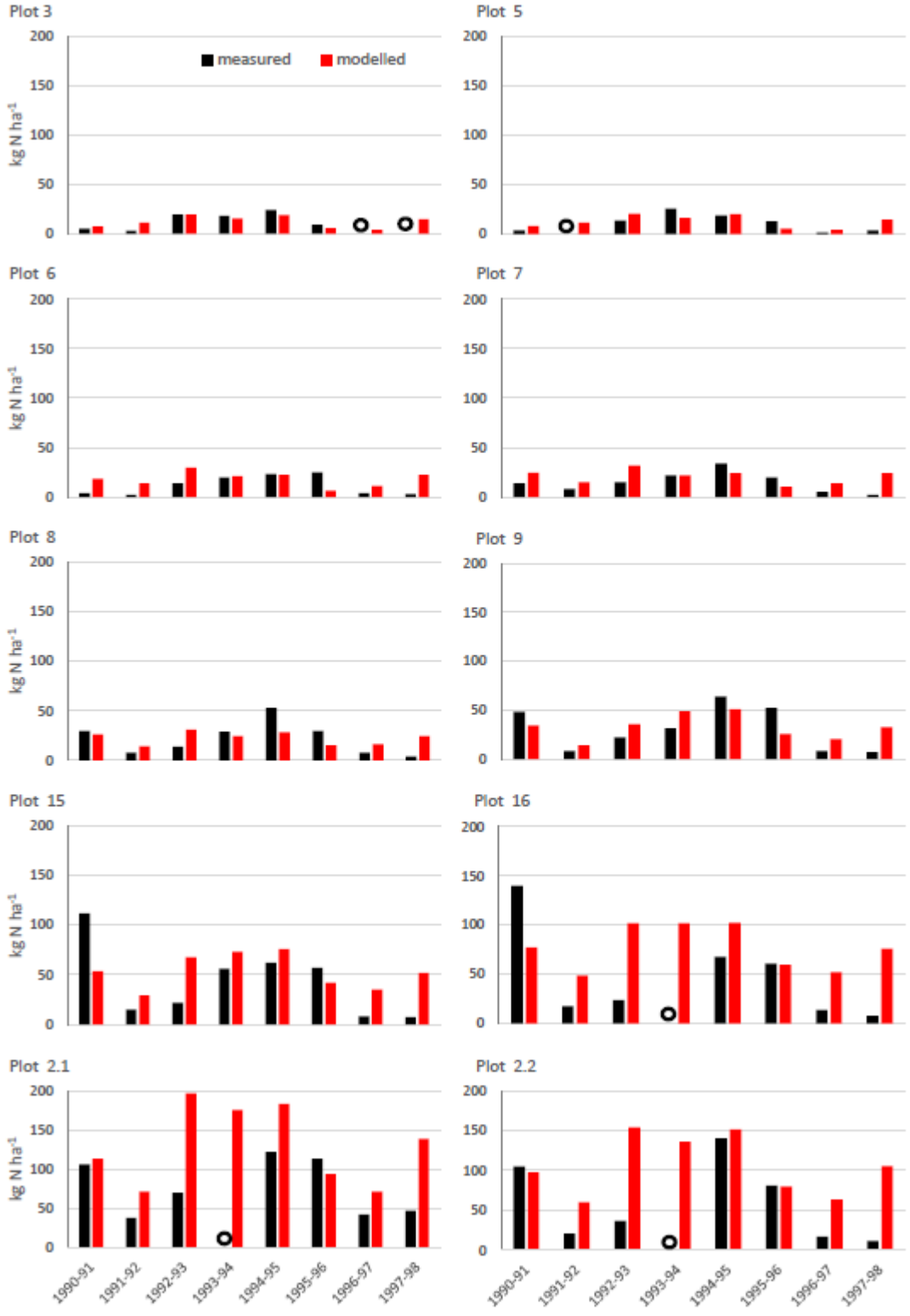

Fig. 8: Estimated and modelled N leached from study plots on the Broadbalk wheat experiment 1990–1998. Measurements are from Section 9 only. The black open circle indicates that no measurement was taken.

657 Table 6 Summary statistics for measured and simulated nitrate leached (kg N ha^{-1} y^{-1}) between

658 1990 and 1998, Broadbalk wheat experiment. Measurements are from Section 9 only.

	Measured		**Simulated**			
Plot no.	Mean kg N ha^{-1} y^{-1}	Standard deviation/ kg N ha^{-1} y^{-1}	Mean kg N ha^{-1} y^{-1}	Standard deviation/ kg N ha^{-1} y^{-1}	RMSE (%)	Correlation
3	13.00	8.51	11.94	5.99	33.29	0.85
5	11.71	8.92	12.86	6.21	58.56	0.60
6	11.88	9.76	18.24	7.38	111.01	-0.02
7	15.00	10.38	20.68	7.01	81.13	0.17
8	22.00	16.55	22.73	6.47	65.70	0.36
9	30.00	22.44	32.74	12.83	57.82	0.58
15	42.38	33.31	53.57	17.51	79.79	0.36
16	47.57	47.02	77.51	22.69	107.32	0.23
2.1	76.86	36.19	130.33	50.46	85.84	0.38
2.2	59.00	50.10	105.98	37.58	103.82	0.45

659

660 *3.2 Park Grass*

661 The model captures the differences between the plots and between the first and second cuts
662 well (Figure 9 and Table 7). The first cut, usually taken in June, is normally higher than the
663 second cut which is usually taken in November).

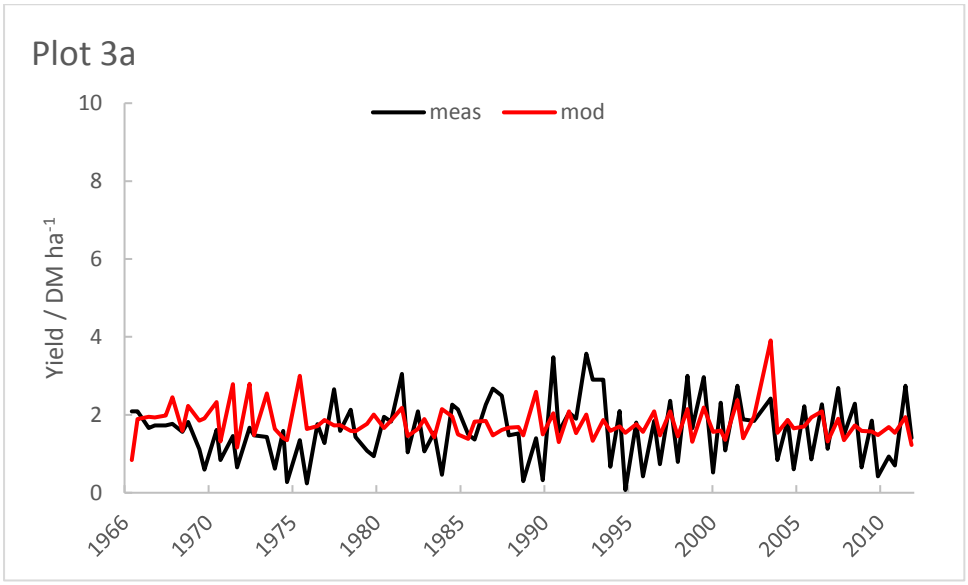

664

665

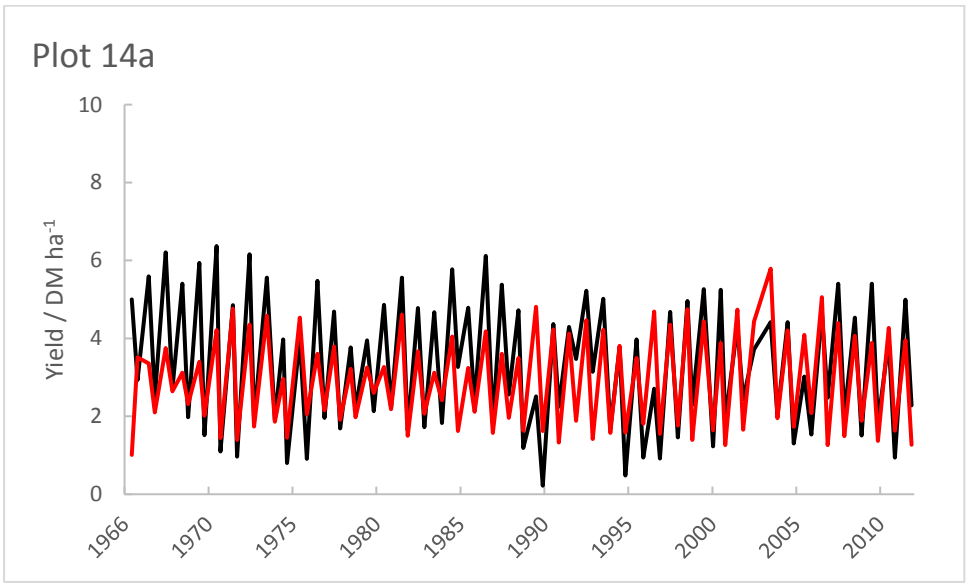

666

667

668 Figure 9 Simulated (red) and measured (black) yields for plots 3a and 14/2a Park Grass
669 permanent grassland experiment, showing both cuts each year.

Table 7 Summary statistics for measured and simulated yield 1966-2012, Park Grass experiment, (47 years, n = 93).

	Measured		**Simulated**			
Plot no.	Mean t ha^{-1}	Standard deviation/ t ha^{-1}	Mean t ha^{-1}	Standard deviation/ t ha^{-1}	RMSE (%)	Correlation
3a	1.61	0.78	1.79	0.43	49.91	0.28
14/2a	3.32	1.67	2.91	1.24	34.35	0.77

3.2 North Wyke Farm Platform

The simulation of water flow rates (m^3 day^{-1}) for catchments 4 and 5 reflect those measured (Fig. 10 and Table 8). This is quantified by the correlations between modelled and measured (Pearson correlation, $r = 0.57$ and $r = 0.55$ respectively). The modelled water flow rate and variation are slightly smaller than the measured in each case.

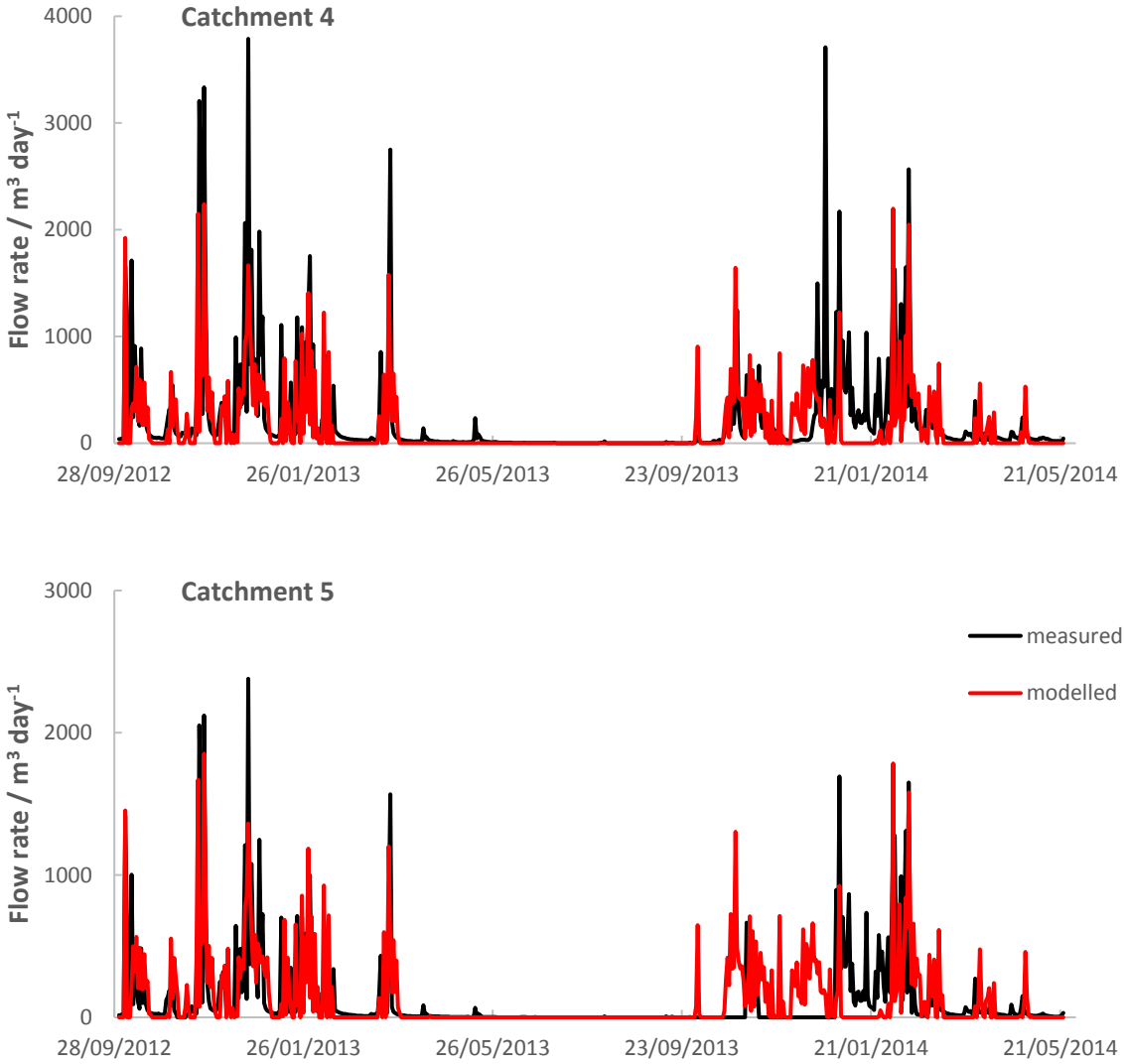

Fig. 10 Simulated (red) and measured (black) flow rates (m^3 day^{-1}) for catchment 4 and 5 of the North Wyke Farm Platform

687 Table 8 Summary statistics for measured and simulated flow and nitrate (kg N per catchment per day) in the drains, North Wyke Farm Platform

688 Catchments 4 and 5.

	Flow (m^3 day^{-1})						**Nitrate (kg N $catchment^{-1}$ day^{-1})**					
	Measured		Simulated				Measured		Simulated			
Catchment	Mean	Std dev	Mean	Std dev	RMSE (%)	Correlation	Mean	Std dev	Mean	Std dev	RMSE (%)	Correlation
4	213.60	457.01	147.83	315.90	180.36	0.57	0.13	0.27	0.47	1.64	1287.69	0.21
5	114.10	281.82	122.88	258.19	226.02	0.55	0.13	0.29	0.01	0.08	248.45	-0.01

689

690

691 The simulation of nitrate in the drainage water over estimates nitrate for catchment 4
692 and under estimates it for catchment 5, but the peaks of nitrate after May 2013 broadly
693 correspond to that which was measured (see Fig. 11 and Table 8).

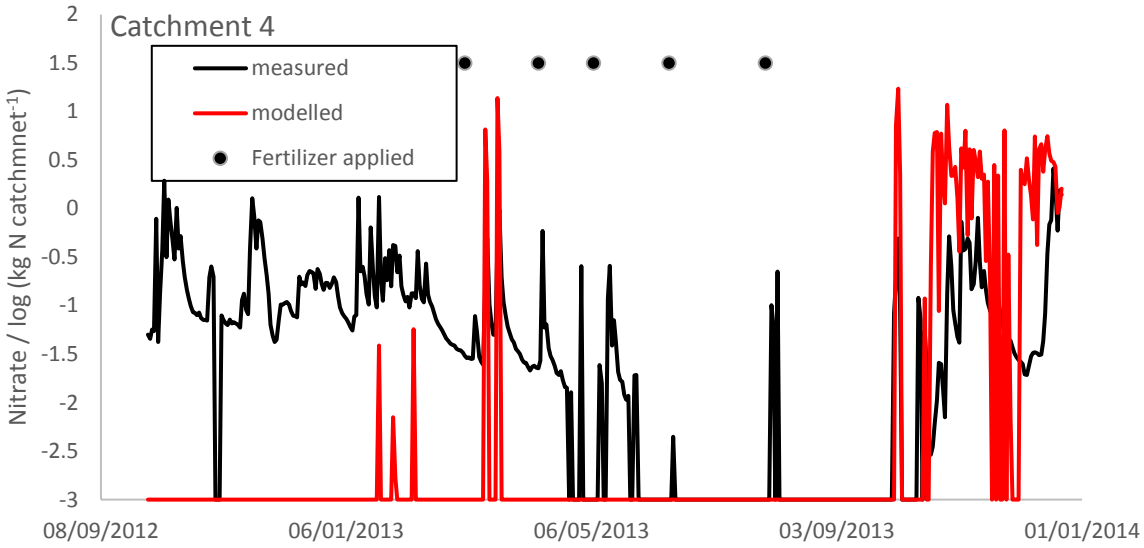

694

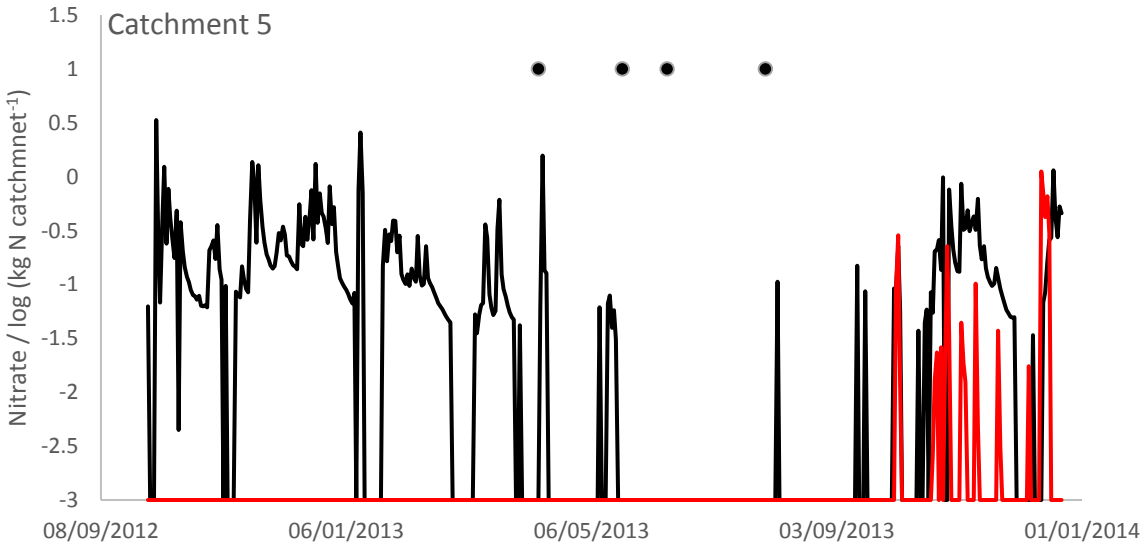

695

696 Fig. 11 Simulated (red line) and measured (black line) log nitrate (kg N /catchment) for
697 catchment 4 and 5 of the North Wyke Farm Platform. The black discs show when nitrogen
698 fertilizer was applied. For details see http://www.rothamsted.ac.uk/farmplatform.

699

3.3 *Trade offs*

By allowing an optimisation algorithm to vary the timing and amount of a single fertilizer application, we identified the trade-offs between yield, nitrate leaching and N_2O emissions for an illustrative example (Fig. 12). The results show that as the yield increases (due to changes in fertilizer application) the lowest possible N_2O emissions that could be achieved simultaneously increases non-linearly. The range of fertilizer N applied to achieve these Pareto optimal objectives was 0 – 210 kg N ha^{-1} y^{-1}. The N_2O emissions reduce as a result of applying less fertilizer later in the growing season. As yield approaches its maximum, both the N_2O emissions and the nitrate leaching increase substantially with increasing amounts of fertilizer for an increasingly marginal improvement in yield. Nitrate leaching and N_2O emissions are synergistic throughout most of the range, however a trade-off appears as the emissions reach their minimum value, as this also results in an increase in leaching. This illustrates how an optimisation approach (e.g. minimising N_2O) could have unitended consequences for another process (nitrate leaching), if both objectives are not considered simultaneously. The optimisation algorithm does not identify a single fertilisation strategy, but highlights nonlinearities thus identifying where a small reduction in one objective could have a large benefit to another. Here, for example, the simulation indicates that the fertilizer application conditions which correspond to a moderate yield, reduce the nitrate that is available to leach from the soil substantially compared to those required for the most yield.

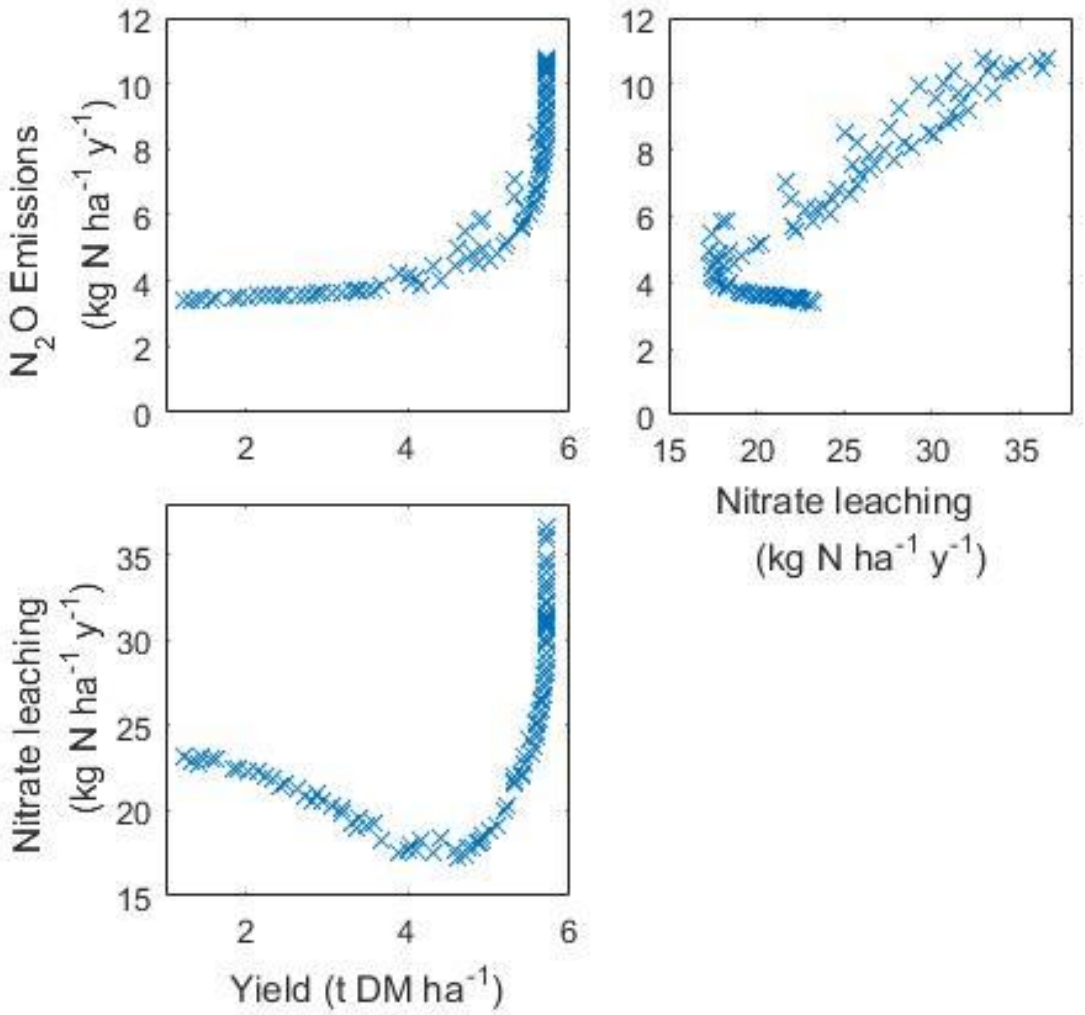

719

720

721 Fig. 12 Illustrative example of use of the model to identify trade-offs between multiple
722 objectives such as maximising yield, minimising nitrate leaching and minimising N_2O
723 emissions. As maximising or minimising any one of these objectives affects the others, the
724 optimisation identifies points on a multi-dimensional frontier with Pareto optimality. On this
725 frontier no objective can be improved upon without a detrimental effect on at least one of the
726 other objectives. This frontier therefore represents the best trade-offs that can be achieved.

727

728

729 **4. Discussion**

730 We have built and used a model framework to simulate spatial and temporal interactions
731 in agricultural landscapes. The framework allows us to explore trade-offs between production
732 and environmental outcomes to determine strategies that could contribute to sustainable food
733 production. It is important that the models reflect the important mechanisms that relate to
734 production and the environment. It is also essential that the models are parsimonious and run
735 quickly so that a large range of scenarios can be tested, perhaps in conjunction with an
736 optimisation algorithm. Our simulations are within 25% of all the observations across multiple
737 years and plots and this is good evidence that the model is robust and that we can use it with
738 confidence to explore trade-offs relevant to farm and environmental management.

739 Simulation of wheat yields from the Broadbalk experiment and grass yields from the
740 Park Grass experiment reproduced both the differences between plots caused by the various
741 fertilizer rates ($\rho > 0.78$) and the observed year-to-year variation (RMSE ranging between
742 20.3 and 28.6% for the mineral N and FYM plots on Broadbalk and 34.3% for Park Grass,
743 correlations were up to 0.77). According to the RMSEs, the model performed less well for the
744 plots that received no fertilizer (plots 3 and 5 on Broadbalk and plot 3a on Park Grass) where
745 the RMSEs were 42.6, 33.4% and 49.9% respectively. The larger values for the RMSE on the
746 lower-yield plots to some extent result from the form of this statistic which is scaled by the
747 reciprocal of the mean observation (i.e. the sum of the squared difference for the lower-yielding
748 plots are scaled by larger values than the higheryielding plots). Over the 46 years that we
749 simulated Broadbalk, the model tended to under predict yield between 1994 and 1996 for plots
750 with higher rates of N fertilizer applied (plots 8, 9, 15, 16, 21, 22) (Fig. 3). This is likely to be
751 a result of excessive water stress when there was no N limitation. It was drier than normal in
752 the three months before harvest in 1994, 1995 and 1996, this led to higher water stress during
753 those months, and so a reduction in dry matter production.

754 The predictions of the variation in grain N for the Broadbalk plots were also good, with
755 the RMSE ranging from 21.3 to 42.5% (Fig. 4, Table 3), and again illustrated the differences
756 between plots receiving different rates of fertilizer N. For P uptake by the crop, the model
757 performed well for most plots with RMSE between 20.2 – 29.0% for all plots except 3 and 5
758 which had RMSE of 89.5% and 48.3% respectively (Fig. 5 and Table 4). In the experiment
759 applications of P stopped in 2001 due to large amounts of plant-available P in the soil, and the
760 P measured in the grain declines noticeably in plots with larger applications of fertilizer but
761 this is not exhibited in the model. However, this does not affect the measured grain yields (Fig
762 3). The variations in simulated yield, grain N and P are approximately 50% smaller than the
763 observed for plots 3 and 5 (for other plots the variation is proportionally more similar). This
764 suggests that the nitrogen stress function maybe over-damping the simulated response to
765 variation in the weather.

766 The modelled total soil organic carbon for the Broadbalk plots fits the measured data
767 well with the RMSE ranging from 3.1 to 13.8% (Fig. 6 and Table 5).

768 The model simulations of N leached from the Broadbalk plots were compared with
769 estimates of leaching from (Goulding et al., 2000), based on nitrate concentrations in drainage
770 and soil water and calculations of drain flow. The measured concentrations of nitrate in soil
771 water were subject to the usual large spatial variation with typical CVs of 50–90%. The
772 simulations reflected the differences in leaching between the different amounts of N, although
773 they tended to overestimate N leached at the largest N rates and in the driest years (Fig. 8 and
774 Table 6). IPCC guidelines (IPCC, 1997;Del Grosso et al., 2005) assume that 30% of applied N
775 is leached or runs off into groundwater or surface waters and this accords with our simulations
776 of Broadbalk where approximately 31.7% of N applied is lost through leaching.

777 The simulation of water flow from the two North Wyke Catchments matches the pattern
778 in the variation of water flow but the average water flow over the simulated periods was larger
779 than that simulated, as was the variation. This suggests that our model system is buffering the
780 water through-put in the catchment and that too much is being taken by the crop or evaporating
781 from the system. The simulations of nitrate in drainage water on the North Wyke plots appeared
782 to be poorer than the simulations of N losses for Broadbalk. Although the timing of peaks in
783 nitrate towards the end of the simulation were determined well, little nitrate was simulated in
784 the first part of the simulated time period. This was because there was very little nitrate left in
785 the model soil profiles at the beginning of the simulated run, and during the summer period
786 (May 2013 – September 2013) there was very little simulated discharge (see Fig. 10). An
787 addition of nitrate on 5th March 2013 to catchment 4 increased the nitrate levels in the soil and
788 a peak in nitrate followed. Further additions of nitrate fertilizer kept the soil nitrate in this
789 simulation at a larger concentration than that in the catchment 5 simulation, which despite
790 having similar levels of nitrate applied, retained less nitrate in the soil. The difference in the
791 simulated soil nitrate between the two catchments manifests as differences in the nitrate in the
792 drainage water in the autumn and winter of 2013 where the nitrate leached was greater for
793 catchment 4 than for catchment 5. The simulated nitrate in the drainage water is larger than
794 that measured for catchment 4 yet smaller for catchment 5. This suggests problems with the
795 modelled uptake of nitrate by the grass and retention in the soil in this case, but we have no
796 explanation for the counter-intuitive discrepancy between the measurements on the two plots.
797 Quantifying the fate of nitrate is notoriously difficult (Senapati et al., 2016). Recently
798 calculated field level budgets of N from the North Wyke platform show unaccounted for losses
799 of between 30 and 60 kg N ha^{-1} (Misselbrook pers. comm.). This highlights the need for more
800 research on the processes that control N transformations from micro-scale to field scale, and
801 larger-scales. Facilities such as the North Wyke farm platform are ideally placed to support

this kinds of research. Models such as the one described here can help to identify the parts of the processes where understanding is incomplete and so can help to inform the design of experiments as well as benefit from any new understanding obtained.

Others have explored trade-offs using empirical data. For example Phalan et al. (2011) compared the effects of land sparing and land sharing on crop yields and the densities of tree and bird species across the UK, while Lamb et al. (2016) explored the need to cut greenhouse gas emissions, while increasing agricultural yields to meet the rapidly rising food demand through land sparing. Eory et al. (2013) examined the trade-offs and synergies between greenhouse gas mitigation measures and other environmental pollutants. The limitation of such empirical studies is that there is a lack of data and so it is often not possible to consider more than two factors at a time. Whilst models should always be used with caution, they do allow us to consider multiple interactions under a large range of management strategies. Used appropriately, models such as the one we present here should allow sound conclusions to be drawn on the relative impact of management strategies and might highlight unintended consequences of certain actions. Whilst the complexity of agricultural systems across the landscape could warrant a complex model, a simpler model that runs more quickly but still captures the key processes can be coupled more easily to an optimisation algorithm. This then provides the opportunity to identify the form of the synergies and trade-offs between multiple objectives at a broad and often neglected scale. Here, for example, we observe that objectives that are largely synergistic such as nitrate leaching and N_2O emissions still exhibit a trade-off as the N_2O emissions approach the minimum. The non-linearity in the leaching and emissions as yield increases is also clear, indicating a strong trade-off.

In order to generate frontiers such as the ones we did here (Fig. 12) an optimisation algorithm must be chosen and a set of management options that the optimisation algorithm can manipulate identified. Within an agricultural landscape, management options are numerous.

For example, even considering only fertiliser applications, the timing, amount and type of multiple applications could all be included in the set of management options to be optimised. This set of options will constrain the frontier, thus care must be taken to identify a reasonable range of options, whilst keeping the number of variables that the algorithm can manipulate to a minimum. Even so, the set of options is likely to represent a complex optimisation problem, involving multiple control variables, with the risk that the algorithm may be trapped in local minima. The optimisation algorithm must be chosen and implemented to minimise this risk. In this case we chose to use non-dominated sorting combined with differential evolution. Whilst the non-dominated sorting allowed us to consider multiple-objectives, which is critical to our aim of generating trade-off curves, the differential evolution combines a genetic algorithm and a gradient based search to allow a complex control space to be explored efficiently.

Our framework includes models of crop growth, the dynamics of soil conditions and water and nutrient flows in order to quantify the trade-offs between agricultural production and environmental factors. It could be expanded to include volatilisation and biological N fixation (which should improve the simulation for certain grass and crop types). Our framework is distinct from alternative models of the agricultural landscape because it simulates multiple functions simultaneously and distinct from other models of ecosystem services (e.g. Sharps et al., 2017) because it focuses on scaling up the effect of field and farm scale management practices to landscape scale. Additional environmental factors are also relevant to the agricultural landscape and to include these the model could be expanded to include weeds, pests and diseases and aspects of biodiversity. For each new component there will be feedbacks into existing models that alter the dynamics of yield accumulation and soil nutrient status. For example, weed population dynamics will depend on the crop and the soil conditions, but in turn weeds will have a competitive effect on the crop, primarily for light, that will affect both yield and to some extent soil nutrient status (Kropff and van Laar, 1993). Our model framework is

spatially explicit and simulates interactions between cells, in particular it describes the lateral flows of nutrients and water from cell to cell based on relative elevation and slope of model cell. The movement of insect pests, for example, is somewhat different as choice of destination are influenced by host plant distribution and the dispersal characteristics of the species in question. It will be straightforward to include these dispersal mechanisms within the landscape framework, see Milne et al. (2015).

Acknowledgements

This research was funded by the Biotechnology and Biological Sciences Research Council (BBSRC) Institute Strategic Programme grant Delivering Sustainable Systems (DSS) and BBSRC ISP Soils 2 Nutrition (S2N), using facilities funded by the BBSRC and also partly by NERC grant NE/J011568/1. We thank P J Gregory for providing root length data, Paul Pulton for soil P data, Jess Evans and Hadewij Sint for help with the North Wyke Farm Platform data, and Chris Watts for providing the soil moisture data. We thank the Lawes Agricultural Trust and Rothamsted Research for data from the e-RA database. The Rothamsted Long-term Experiments National Capability is supported by the BBSRC and the Lawes Agricultural Trust.The North Wyke Farm Platform is a UK National Capability supported by the Biotechnology and Biological Sciences Research Council (BBSRC BB/J004308/1).

References

Addiscott TM, Whitmore AP. Simulation of solute leaching in soils of differing permeabilities. Soil Use and Management 1991; 7: 94-102

875 Andam KS, Ferraro PJ, Pfaff A, Sanchez-Azofeifa GA, Robalino JA. Measuring the
876 effectiveness of protected area networks in reducing deforestation. Proceedings of the
877 National Academy of Sciences of the United States of America 2008; 105: 16089-
878 16094, http://dx.doi.org/10.1073/pnas.0800437105
879 Andrew IKS, Storkey J. Using simulation models to investigate the cumulative effects of
880 sowing rate, sowing date and cultivar choice on weed competition. Crop Protection
881 2017; 95: 109-115, http://dx.doi.org/10.1016/j.cropro.2016.05.002
882 Anon. Sundial-FRS user guide, IACR-Rothamsted and MAFF, 1998, pp. 60
883 Avery BW. Soil classification.for England and Wales (Higher categories). Soil Survey,
884 Technical Monograph No. 14. Rothamsted Experimental Station, Harpenden, England
885 1980, 10.1002/jpln.19811440221
886 Avery BW, Catt JA. The Soil at Rothamsted. Harpenden, Herts: Lawes Agricultural Trust,
887 1995
888 Bell MJ, Jones E, Smith J, Smith P, Yeluripati J, Augustin J, et al. Simulation of soil nitrogen,
889 nitrous oxide emissions and mitigation scenarios at 3 European cropland sites using the
890 ECOSSE model. Nutrient Cycling in Agroecosystems 2012; 92: 161-181,
891 10.1007/s10705-011-9479-4
892 Bell VA, Kay AL, Jones RG, Moore RJ. Development of a high resolution grid-based river
893 flow model for use with regional climate model output. Hydrology and Earth System
894 Sciences 2007; 11: 532-549
895 Boons-Prins ER, de Koning GHJ, van Diepen CA, Penning de Vries FWT. Crop-specific
896 simulation parameters for yield forecasting across the European Community.
897 Simulation Reports CARO-TT, cabo-dlo, 1993
898 Bouman BAM, Schapendonk AHCM, Stol W, van Kraalingen DWG. Description of the
899 grassland growth model LINGRA as implemented in CGMS ab-dlo, 1996

900 Bradbury NJ, Whitmore AP, Hart PBS, Jenkinson DS. Modeling the Fate of Nitrogen in Crop
901 and Soil in the Years Following Application of N-15-Labeled Fertilizer to Winter-
902 Wheat. Journal of Agricultural Science 1993; 121: 363-379
903 Brisson N, Gary C, Justes E, Roche R, Mary B, Ripoche D, et al. An overview of the crop
904 model STICS. European Journal of Agronomy 2003; 18: 309-332,
905 http://dx.doi.org/10.1016/s1161-0301(02)00110-7
906 Colbourn P. The infuence of drainage and cultivation on denitrification losses from an arable
907 clay soil. In: Jenkinson DS, Smith KA, editors. Nitrogen Efficiency in Agricultural
908 Soils. Elsevier Applied Science, England, 1988, pp. 283-294
909 Coleman K, Jenkinson DS. RothC - A Model for the turnover of carbon in soil: Model
910 description and users guide (updated June 2014). Harpenden, UK: Lawes Agricultural
911 Trust, 2014
912 Coleman K, Jenkinson DS, Crocker GJ, Grace PR, Klir J, Korschens M, et al. Simulating trends
913 in soil organic carbon in long-term experiments using RothC-26.3. Geoderma 1997; 81:
914 29-44
915 Cottrill BR, Smith KA. Nitrogen output of livestock excreta. Final report, Defra Project
916 WT0715NVZ, DEFRA, 2007
917 Deb K, Pratap A, Agarwal S, Meyarivan T. A fast and elitist multiobjective genetic algorithm:
918 NSGA-II. Ieee Transactions on Evolutionary Computation 2002; 6: 182-197,
919 http://dx.doi.org/10.1109/4235.996017
920 Del Grosso SJ, Mosier AR, Parton WJ, Ojima DS. DAYCENT model analysis of past and
921 contemporary soil N(2)O and net greenhouse gas flux for major crops in the USA. Soil
922 & Tillage Research 2005; 83: 9-24, http://dx.doi.org/10.1016/j.still.2005.02.007

923 Del Grosso SJ, Parton WJ, Mosier AR, Ojima DS, Kulmala AE, Phongpan S. General model
924 for N2O and N-2 gas emissions from soils due to dentrification. Global Biogeochemical
925 Cycles 2000; 14: 1045-1060
926 Del Prado A, Misselbrook T, Chadwick D, Hopkins A, Dewhurst RJ, Davison P, et al.
927 SIMSDAIRY: A modelling framework to identify sustainable dairy farms in the UK.
928 Framework description and test for organic systems and N fertiliser optimisation.
929 Science of the Total Environment 2011; 409: 3993-4009,
930 http://dx.doi.org/10.1016/j.scitotenv.2011.05.050
931 Eory V, Topp CFE, Moran D. Multiple-pollutant cost-effectiveness of greenhouse gas
932 mitigation measures in the UK agriculture. Environmental Science & Policy 2013; 27:
933 55-67, http://dx.doi.org/10.1016/j.envsci.2012.11.003
934 Feddes RA, Kowalik P, Kolinskamalinka K, Zaradny H. Simulation of field water-uptake by
935 plants using a soil-water dependent root extraction function. Journal of Hydrology
936 1976; 31: 13-26, http://dx.doi.org/10.1016/0022-1694(76)90017-2
937 Gerwitz A, Page ER. An empirical mathematical model to describe plant root systems. Journal
938 of Applied Ecology 1974; 11: 773–781
939 Gil JDB, Reidsma P, Giller KE, Todman LC, Van Ittersum MK. Agriculture, food security and
940 the Sustainable Development Goals: theory and practice in three development contexts.
941 *Global Environmental Change (submitted)* 2017
942 Godwin DC, Allan Jones C. Nitrogen dynamics in soil-plant systems. Modeling pant and soil
943 sytems. ASA-CSSA-SSSA, Madison, 1991
944 Goulding KWT, Poulton PR, Webster CP, Howe MT. Nitrate leaching from the Broadbalk
945 Wheat Experiment, Rothamsted, UK, as influenced by fertilizer and manure inputs and
946 the weather. Soil Use and Management 2000; 16: 244-250

947 Harrod TR, Hogan DV. The Soil of North Wyke and Rowden: North Wyke Research, North
948 Wyke, Devon, 2008
949 IPCC. Intergovernmental panel on climate change guidelines for national greenhouse gas
950 inventories. Agriculture: Nitrous Oxide from Agricultural Soils and Manure
951 Management. OECD, Paris, 1997
952 Jackson B, Pagella T, Sinclair F, Orellana B, Henshaw A, Reynolds B, et al. Polyscape: A GIS
953 mapping framework providing efficient and spatially explicit landscape-scale valuation
954 of multiple ecosystem services. Landscape and Urban Planning 2013; 112: 74-88,
955 http://dx.doi.org/10.1016/j.landurbplan.2012.12.014
956 Keating BA, Carberry PS, Hammer GL, Probert ME, Robertson MJ, Holzworth D, et al. An
957 overview of APSIM, a model designed for farming systems simulation. European
958 Journal of Agronomy 2003; 18: 267-288, http://dx.doi.org/10.1016/s1161-
959 0301(02)00108-9
960 Koh LP, Lee TM, Sodhi NS, Ghazoul J. An overhaul of the species-area approach for
961 predicting biodiversity loss: incorporating matrix and edge effects. Journal of Applied
962 Ecology 2010; 47: 1063-1070, http://dx.doi.org/10.1111/j.1365-2664.2010.01860.x
963 Kropff MJ, van Laar HH. Modelling Crop-weed Interactions: CABI Publishing, 1993
964 Lamb A, Green R, Bateman I, Broadmeadow M, Bruce T, Burney J, et al. The potential for
965 land sparing to offset greenhouse gas emissions from agriculture. Nature Climate
966 Change 2016; 6: 488-492, http://dx.doi.org/10.1038/nclimate2910
967 Lark RM, Milne AE. Boundary line analysis of the effect of water-filled pore space on nitrous
968 oxide emission from cores of arable soil. European Journal of Soil Science 2016; 67:
969 148-159, http://dx.doi.org/10.1111/ejss.12318
970 Li KY, De Jong R, Boisvert JB. An exponential root-water-uptake model with water stress
971 compensation. Journal of hydrology 2001, 252(1), 189-204.

Milne AE, Bell JR, Hutchison WD, van den Bosch F, Mitchell PD, Crowder D, et al. The Effect of Farmers' Decisions on Pest Control with Bt Crops: A Billion Dollar Game of Strategy. Plos Computational Biology 2015; 11, http://dx.doi.org/10.1371/journal.pcbi.1004483

Milne AE, Haskard KA, Webster CP, Truan IA, Goulding KWT, Lark RM. Wavelet analysis of the correlations between soil properties and potential nitrous oxide emission at farm and landscape scales. European Journal of Soil Science 2011; 62: 467-478, http://dx.doi.org/10.1111/j.1365-2389.2011.01361.x

Milne AE, Lark RM, Addiscott TM, Goulding KWT, Webster CP, O'Flaherty S. Wavelet analysis of the scale- and location-dependent correlation of modelled and measured nitrous oxide emissions from soil. European Journal of Soil Science 2005; 56: 3-17, http://dx.doi.org/10.1111/j.1365-2389.2004.00650.x

Monteith JL. Conservative behaviour in the response of crops to water and light. In: Rabbinge R, Goudriaan J, Van Keulen H, Penning de Vries FWT, Van Laar HH, editors. Theoretical Production Ecology: Reflections and Prospects. Pudoc, Wageningen, The Netherlands, 1990, pp. 3-16

Monteith JL, Moss CJ. Climate and the Efficiency of Crop Production in Britain [and Discussion]. Philosophical Transactions of the Royal Society of London B: Biological Sciences 1977; 281: 277-294, 10.1098/rstb.1977.0140

Nömmik H. Investigations on Denitrification in Soil. Acta Agriculturae Scandinavica 1956; 6: 195-228, http://dx.doi.org/10.1080/00015125609433269

Orr RJ, Murray PJ, Eyles CJ, Blackwell MSA, Cardenas LM, Collins AL, et al. The North Wyke Farm Platform: effect of temperate grassland farming systems on soil moisture contents, runoff and associated water quality dynamics. European Journal of Soil Science 2016; 67: 374-385, http://dx.doi.org/10.1111/ejss.12350

997 Parton WJ, Holland EA, Del Grosso SJ, Hartman MD, Martin RE, Mosier AR, et al.
998 Generalized model for NOx and N2O emissions from soils. Journal of Geophysical
999 Research-Atmospheres 2001; 106: 17403-17419,
1000 http://dx.doi.org/10.1029/2001jd900101
1001 Parton WJ, Schime DS, Ojima DS, Cole CV. A general model for soil organic matter dynamics:
1002 sensitivity to litter chemistry, texture and management. In: Bryant RB, Arnold RW,
1003 editors. Quantitative Modeling of Soil Forming Processes. SSSA Special Publication
1004 39, Madison, WI, 1994, pp. 147-167
1005 Phalan B, Onial M, Balmford A, Green RE. Reconciling Food Production and Biodiversity
1006 Conservation: Land Sharing and Land Sparing Compared. Science 2011; 333: 1289-
1007 1291, http://dx.doi.org/10.1126/science.1208742
1008 Rawls WJ. Estimating Soil Bulk-Density from Particle-Size Analysis and Organic-Matter
1009 Content. Soil Science Soil Science 1983; 135: 123-125
1010 Rolston DE, Rao PSC, Davidson JM, Jessup RE. Simulation of denitrification losses of nitrate
1011 fertilizer applied to uncropped, cropped, and manure-amended field plots. Soil Science
1012 1984; 137: 270-279, http://dx.doi.org/10.1097/00010694-198404000-00009
1013 Schapendonk A, Stol W, van Kraalingen DWG, Bouman BAM. LINGRA, a sink/source model
1014 to simulate grassland productivity in Europe. European Journal of Agronomy 1998; 9:
1015 87-100, http://dx.doi.org/10.1016/s1161-0301(98)00027-6
1016 Semenov MA, Jamieson PD, Martre P. Deconvoluting nitrogen use efficiency in wheat: A
1017 simulation study. European Journal of Agronomy 2007; 26: 283-294,
1018 http://dx.doi.org/10.1016/j.eja.2006.10.009
1019 Semenov MA, Stratonovitch P. Adapting wheat ideotypes for climate change: accounting for
1020 uncertainties in CMIP5 climate projections. Climate Research 2015; 65: 123-139,
1021 http://dx.doi.org/10.3354/cr01297

1022 Senapati N, Chabbi A, Giostri AF, Yeluripati JB, Smith P. Modelling nitrous oxide emissions
1023 from mown-grass and grain-cropping systems: Testing and sensitivity analysis of
1024 DailyDayCent using high frequency measurements. Science of the Total Environment
1025 2016; 572: 955-977, http://dx.doi.org/10.1016/j.scitotenv.2016.07.226
1026 Sharpley AN. Depth of Surface Soil-runoff Interaction as Affected by Rainfall, Soil Slope, and
1027 Management1. Soil Science Society of America Journal 1985; 49: 1010-1015,
1028 http://dx.doi.org/10.2136/sssaj1985.03615995004900040044x
1029 Sharps K, Masante D, Thomas A, Jackson B, Redhead J, May L, et al. Comparing strengths
1030 and weaknesses of three ecosystem services modelling tools in a diverse UK river
1031 catchment. Science of the Total Environment 2017; 584: 118-130,
1032 10.1016/j.scitotenv.2016.12.160
1033 Shibu ME, Leffelaar PA, van Keulen H, Aggarwal PK. LINTUL3, a simulation model for
1034 nitrogen-limited situations: Application to rice. European Journal of Agronomy 2010;
1035 32: 255-271, 10.1016/j.eja.2010.01.003
1036 Smith P, Smith JU, Powlson DS, McGill WB, Arah JRM, Chertov OG, et al. A comparison of
1037 the performance of nine soil organic matter models using datasets from seven long-term
1038 experiments. Geoderma 1997; 81: 153-225
1039 Storkey J, Macdonald AJ, Poulton PR, Scott T, Kohler IH, Schnyder H, et al. Grassland
1040 biodiversity bounces back from long-term nitrogen addition. Nature 2015; 528: 401-
1041 404, http://dx.doi.org/10.1038/nature16444
1042 Storn R, Price K. Differential evolution - A simple and efficient heuristic for global
1043 optimization over continuous spaces. Journal of Global Optimization 1997; 11: 341-
1044 359, http://dx.doi.org/10.1023/a:1008202821328

1045 Tilman D, Fargione J, Wolff B, D'Antonio C, Dobson A, Howarth R, et al. Forecasting
1046 agriculturally driven global environmental change. Science 2001; 292: 281-284,
1047 http://dx.doi.org/10.1126/science.1057544
1048 van Genuchten MT. A closed-form equation for predicting the hydraulic conductivity of
1049 unsaturated soils. Soil Science Society of America Journal 1980; 44: 892-898
1050 Van Ittersum MK, Leffelaar PA, Van Keulen H, Kropff MJ, Bastiaans L, Goudriaan J.
1051 Developments in modelling crop growth, cropping systems and production systems in
1052 the Wageningen school. NJAS - Wageningen Journal of Life Sciences 2003; 50: 239-
1053 247, http://dx.doi.org/10.1016/S1573-5214(03)80009-X
1054 van Laar HH, Goudriaan J, van Keulen H. SUCROS97: Simulation of crop growth for potential
1055 and water-limited production situations as applied to spring wheat. Quantitative
1056 Approaches in Systems Analysis. ab-dlo, Netherlands, 1997
1057 Watts CW, Clark LJ, Poulton PR, Powlson DS, Whitmore AP. The role of clay, organic carbon
1058 and long-term management on mouldboard plough draught measured on the Broadbalk
1059 wheat experiment at Rothamsted. Soil Use and Management 2006; 22: 334-341
1060 Whitehead PG, Jin L, Crossman J, Comber S, Johnes PJ, Daldorph P, et al. Distributed and
1061 dynamic modelling of hydrology, phosphorus and ecology in the Hampshire Avon and
1062 Blashford Lakes: Evaluating alternative strategies to meet WFD standards. Science of
1063 the Total Environment 2014; 481: 157-166,
1064 http://dx.doi.org/10.1016/j.scitotenv.2014.02.007
1065 Whitmore AP, Whalley WR, Bird NRA, Watts CW, Gregory AS. Estimating soil strength in
1066 the rooting zone of wheat. Plant and Soil 2011; 339: 363-375,
1067 http://dx.doi.org/10.1007/s11104-010-0588-7

Wolf J. User guide for LINTUL4 and LINTUL4V: Simple generic model for simulation of crop growth under potential, water limited and nitrogen limited conditions Wageningen UR, Wageningen, 2012, pp. 58

Wolf J, de Wit CT, Janssen BH, Lathwell DJ. Modelling long-term crop response to fertilizer phosphorus. I. The model. Agronomy Journal 1987; 79: 445-451

Wösten JHM, Lilly A, Nemes A, Le Bas C. Development and use of a database of hydraulic properties of European soils. Geoderma 1999; 90: 169-185, http://dx.doi.org/10.1016/s0016-7061(98)00132-3